DEMS
Department of Economics, Management and Statistics

DEMS WORKING PAPER SERIES

An epidemiological evolutionary game model with regulation

**Fausto Cavalli, Ahmad Naimzada,
Marina Pireddu**

No. 576 – June 2026

**Department of Economics, Management and Statistics
University of Milano – Bicocca
Piazza Ateneo Nuovo 1 – 2016 Milan, Italy
http://dems.unimib.it/**

An epidemiological evolutionary game model with regulation

Fausto Cavalli, Ahmad Naimzada
Department of Economics, Management and Statistics,
University of Milano - Bicocca, Milano, Italy
fausto.cavalli@unimib.it, ahmad.naimzada@unimib.it

Marina Pireddu
Department of Mathematics and its Applications,
University of Milano - Bicocca, Milano, Italy
marina.pireddu@unimib.it

Abstract

We propose a coevolutionary model linking epidemic dynamics to the strategic choices of agents, in response to decisions by a central regulator. The epidemic is represented by a discrete-time SIS model, with the infection rate endogenously determined by agent strategies. In particular, cooperative and non-cooperative behaviors correspond to low and high infection rates, respectively, and the overall rate is a weighted average based on the population shares adopting each strategy. These shares change with time through an evolutionary selection mechanism, whose fitness measure depends on the epidemic trajectory relative to the agent perceived alert threshold, above which the epidemic situation is considered risky by agents. The regulator influences the alert level based on an ideal target number of infections. The resulting model consists in a three-dimensional discrete-time system, describing the evolution of the epidemiological sector, of the share updating rule and of the alert threshold. We study the resulting interplay both from a static perspective, focusing in particular on the nature of the strategic interaction at both endemic and disease-free steady states, as well as in regard to dynamical features, taking into account out-of-equilibrium trajectories and investigating the possible emergence of multistability phenomena.

Keywords: Epidemiological model; Evolutionary game; Stability; Coexistence; Off-equilibrium dynamics.

JEL Classification: I18, C73, D83, C62

1 Introduction

Since the beginning of the twentieth century, the world has experienced several pandemic events of different nature, duration, and magnitude. We can mention the influenza pandemics, such as the Spanish flu (1918–1920), the Asian flu (1957–1958), and the Hong Kong flu (1968–1969), as well as the AIDS pandemic (beginning in 1981) and the COVID-19 pandemic (2019–2023). However, the latter was the first case in which non pharmaceutical measures to contain the spread of the epidemics, such as lockdowns and social distancing, were introduced on a global scale, especially in the initial phases.[1] Even though these measures were meant to slow down the spread

[1] We refer e.g. to [1] for considerations about the initial implemented non pharmaceutical interventions and their effectiveness.

of infection and prevent healthcare systems from collapsing, they still faced problems and criticism. The economies of many countries were severely strained by lockdowns, with production activities and raw material supply being halted. The mandates that were imposed on populations were not always received with a positive response because of the restrictions on personal freedom they imposed and due to the uncertainties surrounding their actual effectiveness and potential risks (see e.g. [2] for a survey and discussion on social and economic costs). Medical and pharmaceutical research enabled the development of vaccines, which gradually and partially replaced non-pharmaceutical containment and prevention measures. However, even the vaccination campaigns promoted were not always welcomed favorably, as they were accompanied by perplexity or misinformation about the efficacy of the vaccines, leading to "vaccine-hesitancy" ([3]). As stressed in the conclusions of the work by the Lancet commission ([4]), the fundamental pillars for effectively countering a pandemic outbreak (prevention, containment, health services, equity in protecting the most vulnerable individuals, global innovations and their spread) can only be effective within a sufficiently prosocial framework. Such a framework requires both government policies oriented towards the society, and personal willingness to adopt behaviors that reduce the risk of fostering contagion (wearing masks, adhering to isolation when ill, maintaining adequate social distancing, getting vaccinated). The committee's work highlights that the emergence of prosocial behavior is particularly challenging in contexts where choices are shaped by strategic interactions among agents. The rise of non-cooperative, self-interested behavior reduces the effectiveness of the implemented measures and ultimately undermines collective well-being.

Several strands of theoretical research that developed in the aftermath of the pandemic outbreak have focused on combining epidemiological aspects with economic and social ones, recognizing from the very beginning the need for an integrated approach to address the problem. In this regard, we can mention the review study [5], which highlights how the common approach in the literature examining the effect of strategic interactions in epidemiological contexts relies on models that integrate classic compartmental frameworks with decision models. The former ones range from the simple Susceptible-Infected-Susceptible setting introduced in [6] to more elaborated ones (e.g. the susceptible-exposed-infectious-removed SEIR model in [7] and the susceptible-asymptomatic-infectious-unreported symptomatic-isolated-recovered SAIUGR setting proposed in [8]), and aim to model the epidemic dynamical evolution by encompassing simple rules describing the interaction among different states. The coupling of compartmental models with decision-making frameworks has the goal to incorporate human involvement into the biological dynamics of epidemic spread, accounting for both regulatory interventions and the behavioral choices of individuals. In line with the conclusions of the Lancet Commission, we focus on approaches that describe such decision processes through strategic interactions among agents, grounded in a game-theoretic framework [5, 9–11]. Given the very large number of agents typically involved, game-theoretic settings that include an evolutionary selection mechanism are of particular relevance. In this respect, we can mention [12], in which a susceptible–exposed–quarantined–infected–hospitalized–recovered (SEQIHR) epidemiological model is affected by the dynamics arising from a behavioral evolutionary game. The agents can adhere or not to a stay-at-home order depending on the fitness measures related to the perceived payoff of compliance and of the risk of becoming infected through non-compliance. In particular, such risk for the agents when choosing to be non-compliant is weighed against the cost they must bear in implementing a stay-at-home strategy. The model also takes into account the possibility for the government to ease this burden through spending on social programmes. Similarly, in [13], far-sighted agents learn, based on a perturbed best reply mechanism, through an evolutionary process which strategy to choose among vaccination, testing and social activity. In [14] the evolution of the disease is described by a continuous-time SIR model, in which the switching rates between compartments depend on the agents choice to either support or disregard the government response. The probability of switching between two behaviors is described in terms of an evolutionary game. Further developments on the interplay between compartmental dynamics and

evolutionarily selected decision processes can also be found in [15, 16].

The key feature of game-theoretic approaches, and in particular of those grounded on evolutionary theory, is that they describe the epidemiological–social dynamics as a coevolutionary process ([17]), in which strategic choices influence the course of the epidemic, while the epidemic itself induces changes in the behavior of the agents.

The contribution we propose falls within this framework and takes inspiration from [18], whose model consists of a three-dimensional system of ordinary differential equations. Madeo and Mocenni showed the possible transitory alternating phases of epidemic peaks and low infection levels, fostered by the interaction between the human behavior and the disease spread. In particular, the model in [18] consists of a continuous-time susceptible-infected-recovered-susceptible (SIRS) model coupled with replicator dynamics in which the agents choose between complying or not with the rules imposed by a regulator. The payoff corresponding to each strategy depends on the level of the epidemic spread compared to a critical value. This threshold represents the infection level beyond which the epidemic situation is perceived as dangerous, whereas infection rates below it are interpreted as indicating that the outbreak is under control. It is important to remark that the emergence of such a threshold is implicitly shaped by two main factors. The first, emphasized in [18], concerns the policy-maker's objectives, since the threshold acts as a crucial tool for regulatory interventions. In particular, the regulator may affect its level through targeted information campaigns aimed at conveying the actual risks associated with the ongoing public health crisis. The second element relates to how these campaigns are received by the population, so that the threshold ultimately reflects the way the regulator's intentions are interpreted and assimilated by individuals. In the present contribution, we seek to make the process leading to the threshold emergence more explicit by introducing a separate description of these two factors and making the threshold determination endogenous through an adaptive process. In particular the regulator, whose institutional role covers epidemiological and economic matters as well as the reporting on the state of the situation in these respects, determines the alert level to be disclosed to the population. This alert level is the implicit outcome of a trade-off between public health and economic considerations. The population assimilates this information and adjusts its perception of the level of risk based on the target communicated by the regulator and on the number of infected individuals. Namely, for the evolution of the perceived alert threshold we will deal with a smooth adaptive mechanism, depending on the current alert level and on the comparison between the regulator's target and the current epidemic situation. In addition to these differences with [18], concerning the modelling of the epidemics, unlike [18] we consider a discrete-time susceptible-infected-susceptible (SIS) setting. The infection rate, as in [18], is endogenous, since individuals can decide to cooperate (wearing a mask, getting vaccinated, respecting social distances, etc.) or not. In more detail, it is described as an average of the infection rates for cooperating and non-cooperating individuals, weighted with the corresponding population shares in that period. The share of cooperating individuals (and consequently that of defecting individuals) changes over time, depending on the relative average payoffs of the cooperative and defecting strategies via a discrete-time exponential replicator mechanism [19]. More precisely, in each period, the average payoffs of the two strategies are computed taking into account, in addition to the shares of cooperating and defecting individuals, also the various outcomes of the interaction in that period between two players randomly chosen within the population.

Considering the epidemiological sector, the share updating rule, and the dynamics of the alert threshold jointly gives rise to a three-dimensional discrete-time dynamical system, for which both static and dynamical investigations are conducted.

From a static perspective, we observe the emergence of multiple disease-free and endemic equilibrium points, which are characterized in terms of the underlying strategic interactions among agents. These equilibria arise either from non-cooperative behavior, in the prisoner's dilemma, or

from cooperative behavior, in no-conflict and harmony games.[2]
The dynamical analysis indicates that the configuration in which the proportion of infected individuals coincides with the regulator's target cannot always be achieved. Moreover, the specification of target level for the epidemic can substantially shape its evolution, either stabilizing the dynamics or inducing instability. The resulting stability properties depend both on structural conditions intrinsic to each individual sector and on factors arising from the interplay between policy interventions and behavioral responses of the population. In particular, endogenous periodic or chaotic instabilities within the epidemiological domain can induce erratic dynamics in strategic decision-making and behavioral responses. However, these instabilities can be attenuated or fully suppressed through the implementation of appropriately designed regulatory policies. Similarly, the communication of the regulator's decisions and their subsequent assimilation by the population can significantly modify the course of the epidemic, potentially giving rise to quasi-periodic dynamics and recurrent epidemic waves. Therefore, the design of an effective policy must take into account the dynamical richness of the system, which can also be expressed through multistability phenomena, possibly associated with different levels of dynamical complexity, and the consequent path dependence of the resulting outcomes.

The remainder of the manuscript is organized as follows. We introduce the model in Section 2 and we study it from static and dynamical perspectives in Section 3. Numerical simulations are reported in Section 4. Section 5 concludes the work and outlines some possible directions for future research. All proofs are gathered in the Appendix.

2 The model

The model we consider takes inspiration from that proposed in [18]. Dynamics evolve at a discrete-time $t = 0, 1, \dots$ scale. A constant size population of agents, during an epidemic outbreak, can decide *to cooperate* with health authority (e.g. to comply with their directives concerning wearing a mask, getting vaccinated, respecting social distances, etc.) or *not to cooperate*. At each time t the population is then divided into two groups, respectively of *cooperating* agents, corresponding to a variable share ω_t of the whole population, and of *not cooperating* agents, whose share is then $1 - \omega_t$. Agents make their choices in an evolutionary strategic setting, in which the payoff of each choice is also influenced by the share θ_t of infected agents that is perceived as a suitable one for the epidemiological situation, being neither too high, due to the risks connected to health, nor too low, given the economic and personal costs, related to freedom limitation, needed to maintain it. Variable θ_t is affected by a target alert threshold of epidemic spread established by a policy-maker.

In what follows, we describe each model component, highlighting the differences with the setting considered in [18]. We stress that, unlike the model we are going to present, the one studied in [18] was defined on a continuous-time scale.

The epidemiological dynamics

The epidemic outbreak is described by a discrete time SIS model[3] (see e.g. [21])

$$\begin{cases} S_{t+1} = S_t + \gamma I_t - \alpha_t \frac{I_t}{N} S_t \\ I_{t+1} = I_t + \alpha_t \frac{I_t}{N} S_t - \gamma I_t \end{cases} \tag{1}$$

which, given a population composed of N individuals, describes the evolution of the number of susceptible S_t and infected I_t individuals, respectively. In (1) parameter $\gamma \in (0, 1]$ represents

[2] See e.g. [20].

[3] In [18] the epidemiological dynamics are instead described by a SIRS model.

the recovery rate, while α_t is the infection rate at time t, which, differently from the classic SIS model, is endogenized and evolves over time.
Assuming that $S_t + I_t = N$ for every $t \in \mathbb{N}$, the above system reduces to

$$i_{t+1} = i_t(1 - \gamma + (1 - i_t)\,\alpha_t), \tag{2}$$

with $i_t = \frac{I_t}{N}$ for every $t \in \mathbb{N}$.

In addition to the intrinsic epidemic features, the infection rate α_t is determined by the agent behavior. In particular, we suppose that the cooperating (in what follows identified by subscript C) and non-cooperating (NC) behaviors are respectively associated with infection rates α_C and α_{NC}. Due to the more prudent behavior of cooperators, we assume that $0 < \alpha_C < \alpha_{NC}$.

If we identify non-cooperating agents with those refraining from any available measure to prevent the spread of infection, we can infer that α_{NC} essentially corresponds to the intrinsic transmissibility level of the disease, namely to the contact rate in the absence of containment policies. Conversely, if cooperating agents are assumed to adopt all recommended and available mitigation measures, the gap between α_C and α_{NC} reflects the effectiveness and strength of the regulator interventions aimed to limit transmission. This means that, when α_C is substantially lower than α_{NC}, we are in a scenario in which the prevention and containment tools introduced are very effective, whereas the closer α_C is to α_{NC} the weaker the underlying public-health control mechanism is.

On the whole, in every time period, α_t in (2) is obtained as an average of the infection rates for cooperating and not cooperating individuals, weighted with the corresponding shares in that period, and hence it results

$$\alpha_t = \omega_t\alpha_C + (1 - \omega_t)\alpha_{NC} = \alpha_{NC} - \omega_t(\alpha_{NC} - \alpha_C). \tag{3}$$

Note that if all the agents were cooperating (respectively, non-cooperating), we would have $\omega_t = 1$ (respectively, $1 - \omega_t = 1$, namely $\omega_t = 0$) and hence the infection rate would coincide with α_C (respectively, with α_{NC}). Consequently, equation (2) becomes

$$i_{t+1} = i_t[1 - \gamma + (1 - i_t)(\alpha_{NC} - \omega_t(\alpha_{NC} - \alpha_C))]. \tag{4}$$

The evolutionary game

In every time period, the decision of individuals to cooperate or not is based on a comparison between the payoffs of the two strategies. In more detail, similarly to [18], the outcome of the interaction at time t between two players randomly chosen within the population for us is described by the payoff matrix in Table 1. Specifically, following [18], $\mathcal{T}$ *represents the temptation*

	C	NC
C	$1, 1$	$\mathcal{S}_t, \mathcal{T}_t$
NC	$\mathcal{T}_t, \mathcal{S}_t$	$0, 0$

Table 1: Payoff matrix

to defect, while $\mathcal{S}$ *is the "sucker's payoff", embodying the fear to be betrayed by others.*

Since it is always preferable for a player, independently of his/her strategy, to interact with a cooperating individual, for every t we assume

$$\mathcal{S}_t < 1 \quad \text{and} \quad \mathcal{T}_t > 0. \tag{5}$$

Calling $\Pi_{C,t}$ (respectively, $\Pi_{NC,t}$) the average payoff of cooperating (respectively, defecting) individuals at time t, it holds that

$$\Pi_{C,t} = \omega_t + (1-\omega_t)\mathcal{S}_t, \qquad \Pi_{NC,t} = \omega_t \mathcal{T}_t.$$

Depending on the relative average payoffs of the cooperative and defecting strategies, the agents can update over time the strategy they want to adopt, or stick to the strategy they adopted in the previous period. This updating mechanism is described by a classic exponential replicator rule[4] [19, page 79]

$$\omega_{t+1} = M_3(i_t, \theta_t, \omega_t) = \frac{\omega e^{\beta \Pi_{C,t}}}{\omega e^{\beta \Pi_{C,t}} + (1-\omega) e^{\beta \Pi_{NC,t}}} = \frac{\omega_t}{\omega_t + (1-\omega_t) e^{\beta(\Pi_{NC,t} - \Pi_{C,t})}}. \quad (6)$$

where $\beta > 0$ is the intensity of choice parameter of the switching mechanism.

Observe that $M_3(i_t, \theta_t, 0) = 0$ and $M_3(i_t, \theta_t, 1) = 1$ for all values of i_t and θ_t. Consequently, homogeneous populations consisting exclusively of cooperating agents or exclusively of non-cooperating agents invariably constitute steady states of the evolutionary dynamics, in accordance with the imitative component embedded within the replicator mechanism.

We note that if the average payoffs of the two strategies coincide, each agent does not change the previous period strategy. The limit case of a null intensity of choice corresponds to a similar situation in which each agent does not modify the initial strategy, independently of the payoffs. Conversely, as β raises, the strategy with the highest average payoff is chosen by an increasingly large share of agents. In the limit case of $\beta \to +\infty$, if $\Pi_{NC,t} > \Pi_{C,t}$ all the agents choose NC strategy, while all the agents adopt C strategy when $\Pi_{NC,t} < \Pi_{C,t}$.

As concerns the ruling quantities $\mathcal{T}_t$ and $\mathcal{S}_t$, similar to [18], we assume that they vary in time depending on the perception by individuals of the strength of the infection, which can be measured by the number or share of infected individuals. Specifically, in the continuous-time setting in [18], $\mathcal{T}_t$ and $\mathcal{S}_t$ are defined, except for a slightly different notation, as follows

$$\mathcal{T}_t = 1 - \tau^0 (I_t - \tilde{\theta}), \qquad \mathcal{S}_t = -\sigma^0 (I_t - \tilde{\theta}), \quad (7)$$

where $\sigma^0 < 0 < \tau^0$ and $\tilde{\theta} \in (0, N)$ are exogenous parameters. In particular, σ^0 and τ^0 are reactivity parameters, while $\tilde{\theta}$ represents an appropriate level of infected agents and thus, it corresponds to the *perceived alert threshold*. When I_t exceeds $\tilde{\theta}$, the agents believe that the epidemic situation is risky, related e.g. to the severity of the disease. This also implies that a low value for $\tilde{\theta}$ means that the agents evaluate the epidemic spread as worrying even for small shares of infected population. Conversely, a large $\tilde{\theta}$ depicts a situation in which the agents believe that the health situation is under control even for large values of I_t.

Recalling that $i_t = \frac{I_t}{N}$, setting $\tau := \tau^0 N$, $\sigma := \sigma^0 N$ and $\theta := \frac{\tilde{\theta}}{N}$, we can rewrite $\mathcal{T}_t$ and $\mathcal{S}_t$ in (7) as

$$\mathcal{T}_t = 1 - \tau(i_t - \theta), \qquad \mathcal{S}_t = -\sigma(i_t - \theta), \quad (8)$$

so that they now depend on i_t rather than on I_t.
Instead of taking θ as exogenous like in [18], we consider it as an endogenous time-varying variable, still describing the perceived alert threshold, above which the epidemic situation is considered risky by agents. Accordingly, rather than with $\mathcal{T}_t$ and $\mathcal{S}_t$ as in (8), we will deal with

$$\mathcal{T}_t = 1 - \tau(i_t - \theta_t), \qquad \mathcal{S}_t = -\sigma(i_t - \theta_t), \quad (9)$$

without changing notation for the ruling quantities, for simplicity's sake. Still for simplicity, we stick to a linear formulation for $\mathcal{T}_t$ and $\mathcal{S}_t$, with $\mathcal{T}_t$ being decreasing with $i_t - \theta_t$, and $\mathcal{S}_t$ being

[4] We recall that in [18] the shares of cooperating and defecting individuals evolve according to a continuous time replicator rule (cf. [22]), in which the average payoffs of the two strategies are contrasted with the average payoff of the whole population.

$\mathcal{S}_t < 0 < 1 < \mathcal{T}_t$

	C	NC
C	$1, 1$	$-0.2, 1.2$
NC	$1.2, -0.2$	$0, 0$

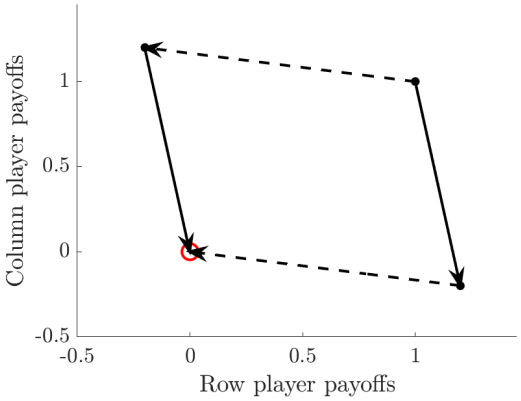

Table 2: Prisoner's dilemma

increasing with $i_t - \theta_t$, quantity which can be taken as a measure of the perceived epidemics severity, given the perceived alert threshold θ_t. Namely, focusing on $\mathcal{T}_t$, i.e., on the temptation to defect, it falls when the epidemic situation is considered more risky, that is, with a raise in $i_t - \theta_t$. In particular, the worst possible scenario in terms of cooperation is when defecting looks very convenient, i.e., when $\mathcal{S}_t < 0 < 1 < \mathcal{T}_t$, and the game corresponds to the prisoner's dilemma, where (NC, NC) is the unique Nash equilibrium. In order to make steady states feasible (i.e., respecting (5)) and to avoid overreaction phenomena, we assume $|\sigma|, \tau \in (0, 1)$. Under such assumptions, in addition to the prisoner's dilemma game, the ranking between $\mathcal{S}_t$ and 0, as well as the one between $\mathcal{T}_t$ and 1, give rise just to other two types of games, in both of which $\mathcal{S}_t$ and $\mathcal{T}_t$ belong to the interval $(0, 1)$. In particular, if $0 < \mathcal{S}_t < \mathcal{T}_t < 1$ the no-conflict game arises, while if $0 < \mathcal{T}_t < \mathcal{S}_t < 1$ the harmony game emerges. Despite the different ranking between $\mathcal{S}_t$ and $\mathcal{T}_t$, the two games display non-conflictual outcomes, having (C, C) as unique Nash equilibrium, since the difference between $\mathcal{S}_t$ and $\mathcal{T}_t$ is not excessive. Indeed, both the no-conflict game and the harmony game are characterized by a loss associated with defection. However, in the no-conflict game such loss (both passing from *CC* to *CD*, and from *CD* to *DD*, as well as in the symmetrical situations) is smaller than in the harmony game. Hence, the no-conflict game is characterized by a weaker push toward cooperation than the harmony game.
In Tables 2-4 we report an example for each possible situation.[5]

The evolution of the perceived alert threshold

We assume that at each time period the agents adapt their perceived alert threshold θ based on their current perceived alert threshold and the discrepancy between a target infection level i_R, communicated by the regulator, and the current infection level, i_t. The regulator intervention has the aim of maintaining the spread of the epidemic at a certain level, and this is encompassed in the target share of infected individuals i_R. The choice of i_R arises from a (not explicitly modeled) trade-off between public health and economic considerations by the regulator. We just say that, for example, in the presence of a disease that is not particularly alarming, i_R may be chosen

[5]Dots represent strategies, with the red one denoting the Nash equilibrium. Solid lines link alternatives available to a row player given the choice of the column one, while dashed lines link alternatives available to a column player given the choice of the row one. Arrows point toward the preferred choice between a couple; in any case, a column player always prefers the strategy characterized by the highest point, while a row player always prefers the strategy characterized by the rightmost point. For more details about representing 2×2 games, we refer to [20].

$0 < \mathcal{S}_t < \mathcal{T}_t < 1$

	C	NC
C	$1, 1$	$0.2, 0.8$
NC	$0.8, 0.2$	$0, 0$

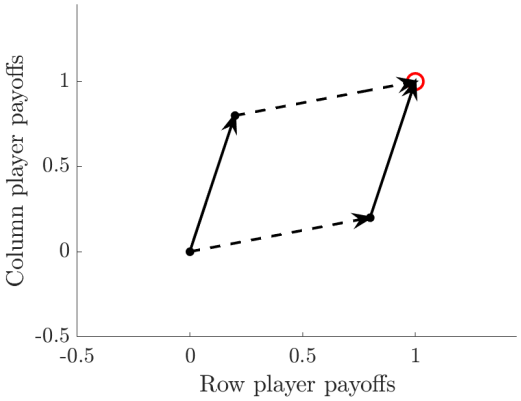

Table 3: No-conflict game

$0 < \mathcal{T}_t < \mathcal{S}_t < 1$

	C	NC
C	$1, 1$	$0.8, 0.2$
NC	$0.2, 0.8$	$0, 0$

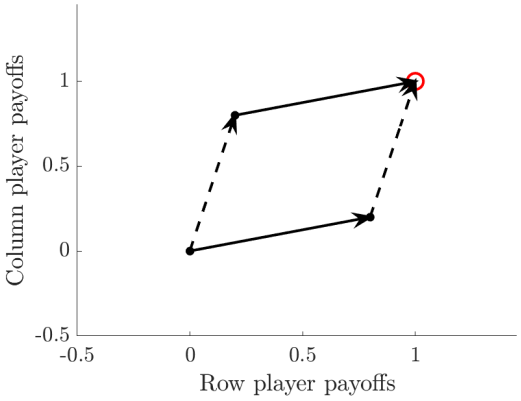

Table 4: Harmony game

appropriately large, while to keep under control a potentially deadly or pandemic spread a low level of infected people may be necessary.

More precisely, as regards the dependence of θ_{t+1} on $i_R - i_t$, for $\theta_t \in (0, 1)$, we need that θ_{t+1} is larger than θ_t, implying a more relaxed mood within the population, if and only if i_t is not too high, lying below the target i_R of the regulator. Namely, when the situation is not considered critical ($i_R > i_t$), the regulator has no reason to maintain heightened vigilance. Consequently, the communication effort on the population is relaxed, leading to a higher level of infection perceived as critical. On the other hand, when $i_R < i_t$, the actual epidemic situation is worse than that described by the target, and therefore the regulator aims at increasing the level of vigilance among the population, and this decreases θ_t. In contrast, θ_t does not change when $i_R = i_t$. However, note that the effect exerted by the sign of $i_R - i_t$ vanishes for $\theta_t = 0$ when $i_R - i_t < 0$, which means that even if the epidemiological situation would lead to a decrease of the alert threshold, the latter being already the one encompassing the highest alert level, it cannot further decrease, and thus $\theta_{t+1} = 0$. A symmetric situation occurs for $\theta_t = 1$ when $i_R - i_t > 0$. In this case, even if the current situation is better than that aimed at by the regulator, the alert level is the minimum possible and the alert threshold cannot increase, so that $\theta_{t+1} = 1$.

We stress that θ_{t+1}, in addition to being influenced by the objective of the regulator, is also affected by the communication channels used and by the population's reception of the conveyed information. In more detail, as concerns the dependence of θ_{t+1} on θ_t, we emphasize that, since the perceived alert threshold lies in $[0,1]$, its scope for variation must shrink as θ_t approaches the interval boundaries. Namely, on the one hand, as θ_t increases, the potential for further upward adjustments diminishes; in the limiting case $\theta_t = 1$, the perceived alert threshold can remain constant or decrease, but cannot increase further. In contrast, as θ_t decreases, the room for further downward adjustments diminishes; in the limiting case $\theta_t = 0$, the perceived alert threshold can only remain constant or increase.

Such an adaptive mechanism can be modelled as

$$\theta_{t+1} = M_2(i_t, \theta_t, \omega_t) = \theta_t + F_2(\theta_t, \rho(i_R - i_t)), \tag{10}$$

where $\rho > 0$ is a reactivity parameter. Note that the evolution of θ depends only on the previous perceived alert threshold and on the comparison between the regulator's target and the current epidemiological situation, without directly depending on the distribution of strategies.

To define a function F_2 that encapsulates the desired behavior while preserving a smooth reaction of the agents to the signal $i_R - i_t$, we can proceed as follows. Consider a smooth, strictly increasing function $f_0 : [0,1] \to [0,1]$, $z \mapsto f_0(z)$, such that $f_0(0) = 0$, $f_0(1) = 1$ and $f_0'(0) = f_0'(1) = 0$, and let us introduce

$$F_2(\theta, z) = \begin{cases} -\theta & z < -f_0^{-1}(\theta) \\ f_0(z + f_0^{-1}(\theta)) - \theta & z \in [-f_0^{-1}(\theta), 1 - f_0^{-1}(\theta)] \\ 1 - \theta & z > 1 - f_0^{-1}(\theta) \end{cases} \tag{11}$$

For example, it is possible to choose

$$f_0(z) = 4z^2 \left(1 - \frac{z}{2}\right)^2, \tag{12}$$

so that $f_0(z) = \theta$ provides

$$f_0^{-1}(\theta) = 1 - \sqrt{1 - \sqrt{\theta}}\,, \tag{13}$$

and thus

$$F_2(\theta, z) = \begin{cases} -\theta & z < -1 + \sqrt{1 - \sqrt{\theta}} \\ \left(\left(z - \sqrt{1 - \sqrt{\theta}}\right)^2 - 1\right)^2 - \theta & z \in \left[-1 + \sqrt{1 - \sqrt{\theta}}, \sqrt{1 - \sqrt{\theta}}\right] \\ 1 - \theta & z > \sqrt{1 - \sqrt{\theta}} \end{cases} \tag{14}$$

for which we have the function whose graph is reported in Figure 1. Note that, thanks to the smoothness of (14), the reaction to $z = \rho(i_R - i_t)$ vanishes as it approaches the values $-1 + \sqrt{1 - \sqrt{\theta}}$ and $\sqrt{1 - \sqrt{\theta}}$, that is, when $\theta + F_2(\theta, z)$ is close to 0 and 1, respectively. We stress that the preceding example may appear somewhat contrived. However, mathematically simpler alternatives would either fail to represent a smooth adjustment of agents to signal $i_R - i_t$ (as it would be the case, for instance, with a linear function interpolating between the two constant segments), or would generate lock-in states from which the system cannot escape. The latter happens, for instance, with a sigmoidal specification of the form $\theta_t \left(-1 + \frac{1}{\theta_t + (1-\theta_t)e^{-\rho(i_R - i_t)}}\right)$, for which it is straightforward to verify that, when $\theta_t = 0$ or $\theta_t = 1$, the perceived level of alert remains fixed and cannot change (see [23] for further details).

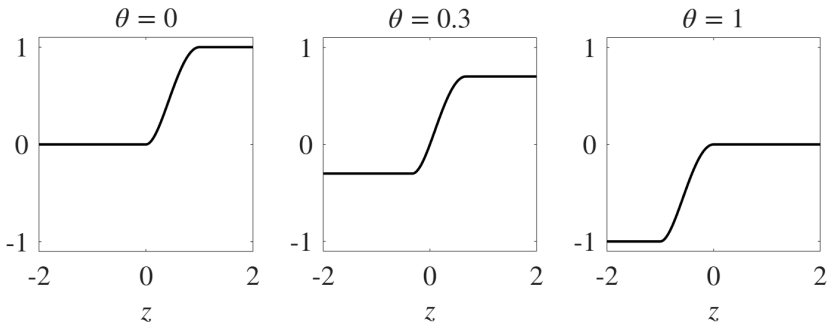

Figure 1: Function F_2, as defined in (14), evaluated for different values of parameter θ.

Gathering (4), (6) and (10), the model defined by $\boldsymbol{M} : [0,1]^3 \to [0,1]^3, (i_t, \theta_t, \omega_t) \mapsto \boldsymbol{M}(i_t, \theta_t, \omega_t)$ where

$$\boldsymbol{M}(i_t,\theta_t,\omega_t) = \begin{cases} i_{t+1} = M_1(i_t,\theta_t,\omega_t) = i_t[1-\gamma+(1-i_t)(\alpha_{NC}-(\alpha_{NC}-\alpha_C)\omega_t)] \\ \theta_{t+1} = M_2(i_t,\theta_t,\omega_t) = \theta_t + F_2(\theta_t, \rho(i_R - i_t)) \\ \omega_{t+1} = M_3(i_t,\theta_t,\omega_t) = \dfrac{\omega_t}{\omega_t + (1-\omega_t)e^{\beta(i_t-\theta_t)(\sigma-\omega_t(\tau+\sigma))}} \end{cases} \tag{15}$$

in which F_2 must be replaced by the expression in (14), in which we recall that γ, ρ, β are positive parameters, $0 < \alpha_C < \alpha_{NC}$, $i_R \in (0,1)$ and $-1 < \sigma < 0 < \tau < 1$. More precisely, in agreement with [21], we assume $\gamma \leq 1$ and

$$\alpha_C,\, \alpha_{NC} \in \left(0, (1+\sqrt{\gamma})^2\right), \tag{16}$$

so that also $\alpha_t \in \left(0, \left(1+\sqrt{\gamma}\right)^2\right)$, conditions under which the positivity of the trajectories is guaranteed. We will consider them starting from Subsection 3.2, in the steady state stability investigation.

3 Mathematical analysis

In this section, we focus on the analysis of the model, first from a static perspective (in Subsection 3.1) and subsequently from a dynamical one (in Subsection 3.2). As a benchmark for comparison, we consider the classic SIS model which, recalling, for instance [21], admits two equilibrium points: an *endemic equilibrium* given by

$$i^* = 1 - \frac{\gamma}{\alpha},$$

which exists whenever $\gamma < \alpha$, and a *disease-free equilibrium*

$$i_0^* = 0,$$

which exists for all parameter values. In analogy with this, we separately study steady states of (15) characterized by a null or positive level of infected agents, addressing them as disease-free or endemic steady states.

3.1 Static analysis

We investigate possible steady states of model (15), focusing on disease-free steady states in Proposition 1 and on endemic ones in Proposition 2.

Proposition 1. *The steady states* $(i^*, \theta^*, \omega^*)$ *of* (15) *characterized by* $i^* = 0$ *are those listed in the following table.*

Disease-free steady states
$\boldsymbol{\xi}^*_{df} = (0, 1, 0)$
$(0, 1, 1)$

According to Proposition 1, differently from the classic SIS model, System (15) does not exhibit a unique disease-free steady state, even if we disclose in advance that the only potentially stable one is $\boldsymbol{\xi}^*_{df}$, while $(0, 1, 1)$ is always unstable. Note that $\boldsymbol{\xi}^*_{df}$ consists of a population of non-cooperating agents with a null concern of the epidemic, which is quite predictable and natural since no disease is present.

Proposition 2. *The steady states* $(i^*, \theta^*, \omega^*)$ *of* (15) *characterized by* $i^* > 0$ *are those listed in the following table.*

Endemic steady state	*Existence condition*
$\boldsymbol{\xi}^*_R = \left(i_R, i_R, \frac{\alpha_{NC} - \frac{\gamma}{1-i_R}}{\alpha_{NC} - \alpha_C}\right)$	$(1 - i_R)\alpha_C < \gamma < (1 - i_R)\alpha_{NC}$
$\boldsymbol{\xi}^*_C = \left(1 - \frac{\gamma}{\alpha_C}, 0, 1\right)$	$\gamma < (1 - i_R)\alpha_C$
$\boldsymbol{\xi}^*_{NC} = \left(1 - \frac{\gamma}{\alpha_{NC}}, 1, 0\right)$	$(1 - i_R)\alpha_{NC} < \gamma < \alpha_{NC}$
$\left(1 - \frac{\gamma}{\alpha_C}, 1, 1\right)$	$(1 - i_R)\alpha_C < \gamma < \alpha_C$
$\left(1 - \frac{\gamma}{\alpha_{NC}}, 0, 0\right)$	$\gamma < (1 - i_R)\alpha_{NC}$
$\tilde{\boldsymbol{\xi}}^*_C = (i_R, \theta, 1),\ \forall \theta \in [0, 1]$	$\begin{cases} \gamma < \alpha_C \\ i_R = 1 - \frac{\gamma}{\alpha_C} \end{cases}$
$\tilde{\boldsymbol{\xi}}^*_{NC} = (i_R, \theta, 0),\ \forall \theta \in [0, 1]$	$\begin{cases} \gamma < \alpha_{NC} \\ i_R = 1 - \frac{\gamma}{\alpha_{NC}} \end{cases}$

Concerning endemic situations too, differently from the isolated SIS model, System (15) exhibits several endemic steady states by Proposition 2.

In particular, steady state $\boldsymbol{\xi}^*_R$ is characterized by an epidemic spread that coincides with the goal of the regulator, and the perceived threshold of alert exactly mirrors that encompassed in the regulator target. Recalling that an endemic steady state of the SIS model must fulfill condition $i^* = 1 - \frac{\gamma}{\alpha}$, it is immediate to see that $\frac{\gamma}{1-i_R}$ is the contact rate that realizes such an identity for $i^* = i_R$. As a further confirmation of this, it is possible to verify that the steady state distribution of shares, with $\omega^* = \omega^*_R := \frac{\alpha_{NC} - \frac{\gamma}{1-i_R}}{\alpha_{NC} - \alpha_C}$, is such that the resulting average contact rate (3) is $\frac{\gamma}{1-i_R}$. The existence condition for $\boldsymbol{\xi}^*_R$ is then evident. Namely, $i^* = i_R$ can be achieved only if the distribution of shares allows for a contact rate $\frac{\gamma}{1-i_R}$, which is possible only if it lies between the contact rates characterizing the two extremal homogeneous populations consisting just of cooperating or of non-cooperating agents. We stress that $\boldsymbol{\xi}^*_R$ is the only state in which the population contains both cooperating and non-cooperating agents. As recalled in Section 2, $\omega = 0$ and $\omega = 1$ are steady states as a consequence of the replicator evolutionary dynamics, in addition to any configuration in which cooperating and non-cooperating agents earn the same profit, which is precisely the case at $\boldsymbol{\xi}^*_R$.

The next two steady states $\boldsymbol{\xi}^*_C$ and $\boldsymbol{\xi}^*_{NC}$ respectively correspond to equilibria characterized by a homogeneous population, either of cooperators or of non-cooperators, with a share of infected individuals consistent with the respective contact rate α_C or α_{NC}.

Carrying on the overview of the endemic steady states, $\left(1-\frac{\gamma}{\alpha_C},1,1\right)$ and $\left(1-\frac{\gamma}{\alpha_{NC}},0,0\right)$ closely resemble $\boldsymbol{\xi}_C^*$ and $\boldsymbol{\xi}_{NC}^*$, respectively, and just differ from them for the steady perceived alert threshold. We avoided to label them since, disclosing in advance a result from the dynamical analysis (see Proposition 6), these steady states are always unstable for model (15).

Finally, we have the two continua of steady states $\tilde{\boldsymbol{\xi}}_C^*$ and $\tilde{\boldsymbol{\xi}}_{NC}^*$, each of which occurs for a very particular regulator's goal i_R. The reason why endemic steady states $\tilde{\boldsymbol{\xi}}_C^* = (i_R, \theta, 1)$, with $i_R = 1-\frac{\gamma}{\alpha_C}$, and $\tilde{\boldsymbol{\xi}}_{NC}^* = (i_R, \theta, 0)$, with $i_R = 1-\frac{\gamma}{\alpha_{NC}}$, for all $\theta \in [0,1]$ form a continuum of equilibria characterized by "indifference" with respect to θ is understood by inspecting the drivers leading to the formation of steady states $\boldsymbol{\xi}_C^*$, $\boldsymbol{\xi}_{NC}^*$, and $\boldsymbol{\xi}_R^*$. The "regulator equilibrium" $\boldsymbol{\xi}_R^*$ associated with a mixed population share $\omega^* \in (0,1)$ does not exhibit indifference with respect to θ, since under the evolutionary replicator dynamics the coexistence of both strategies is preserved. The payoff comparison between $\Pi_{C,t}$ and $\Pi_{NC,t}$ induces an internal selection pressure that modifies the epidemiological dynamics and uniquely determines $\theta^* = i_R$. The operative evolutionary dynamics inhibits complete polarization, thereby ensuring that the threshold remains constrained by persistent processes of strategic competition. Conversely, the homogeneous population steady states $\boldsymbol{\xi}_C^* = (1-\frac{\gamma}{\alpha_C}, 0, 1)$ and $\boldsymbol{\xi}_{NC}^* = (1-\frac{\gamma}{\alpha_{NC}}, 1, 0)$ arise when $i^* \neq i_R$, thus a nonzero regulatory signal induces a persistent structural tension in the system. Such signal actively drives toward a unique steady-state configuration: $\theta^* = 0$ (corresponding to maximum alert) when $i^* > i_R$ (the fully cooperative regime) and $\theta^* = 1$ (corresponding to minimum alert) when $i^* < i_R$ (the fully non-cooperative regime). The threshold value is thus identified and stabilized by the sustained action of the regulatory pressure.

At $\tilde{\boldsymbol{\xi}}_C^*$ and $\tilde{\boldsymbol{\xi}}_{NC}^*$, both these pushes cease to work. There is no regulatory pressure, since the target infection level coincides exactly with the natural endemic level: $i_R = 1-\frac{\gamma}{\alpha_C}$ (for $\tilde{\boldsymbol{\xi}}_C^*$) or $i_R = 1-\frac{\gamma}{\alpha_{NC}}$ (for $\tilde{\boldsymbol{\xi}}_{NC}^*$), and therefore the signal $z = \rho(i_R - i_t)$ induced by the regulator vanishes ($z = 0$). Moreover, the population is already polarized ($\omega = 1$ or $\omega = 0$), so there is no evolutionary pressure that contributes to promote values of θ by altering the evolution of the epidemic. The system enters a region characterized by indifference with respect to θ, which is then indeterminate. The initial perceived alert threshold is driven by the strength of the regulatory pressure or by the evolutionary mechanism during the transient dynamics out-of-equilibrium, but once these two drivers lose their strength, the trajectories remain close to a value of θ that actually depends only on the initial status of the system.

In any case, the conditions required for the emergence of such steady states are so restrictive that their practical significance is limited. Consequently, we will not undertake a detailed analysis of them in the subsequent discussion.

Looking also at the existence conditions in Proposition 2, we stress that $\tilde{\boldsymbol{\xi}}_C^*$ plays the role of a transitional steady state between $\boldsymbol{\xi}_C^*$ and $\boldsymbol{\xi}_R^*$ as i_R increases, and, symmetrically, $\tilde{\boldsymbol{\xi}}_{NC}^*$ plays the role of a transitional steady state between $\boldsymbol{\xi}_R^*$ and $\boldsymbol{\xi}_{NC}^*$ as i_R increases. Indeed, in our investigations in Subsection 3.2 and, mainly, in Section 4 we will study the effect obtained by varying with continuity i_R, ρ and β, while the value of the other parameters defines the configuration under analysis.

We analyze in Propositions 3 and 4 which kind of games can emerge at disease-free and endemic steady states.

Proposition 3. *The disease-free steady states reported in Proposition 1 lead to the following games:*

Disease-free steady state	*Steady state payoff matrix*			*Steady state game types*
$\boldsymbol{\xi}^*_{df}$		*C*	*NC*	*PD*
	C	$1,1$	$\in (-1,0)\times(1,2)$	
	NC	$\in (1,2)\times(-1,0)$	$0,0$	
$(0,1,1)$		*C*	*NC*	*PD*
	C	$1,1$	$\in (-1,0)\times(1,2)$	
	NC	$\in (1,2)\times(-1,0)$	$0,0$	

The only game emerging at disease-free steady states is, as expected, the prisoner's dilemma, due to the lack of infection and the consequent convenience of defecting.

Proposition 4. *The endemic steady states reported in Proposition 2 lead to the following games:*

Endemic steady state	*Steady state payoff matrix*			*Steady state game types*
$\boldsymbol{\xi}^*_R$		*C*	*NC*	*PD-NoCG (limit case)*
	C	$1,1$	$0,1$	
	NC	$1,0$	$0,0$	
$\boldsymbol{\xi}^*_C$		*C*	*NC*	*NoCG or HG*
	C	$1,1$	$\in (0,1)^2$	
	NC	$\in (0,1)^2$	$0,0$	
$\boldsymbol{\xi}^*_{NC}$		*C*	*NC*	*PD*
	C	$1,1$	$\in (-1,0)\times(1,2)$	
	NC	$\in (1,2)\times(-1,0)$	$0,0$	
$\left(1-\frac{\gamma}{\alpha_C},1,1\right)$		*C*	*NC*	*PD*
	C	$1,1$	$\in (-1,0)\times(1,2)$	
	NC	$\in (1,2)\times(-1,0)$	$0,0$	
$\left(1-\frac{\gamma}{\alpha_{NC}},0,0\right)$		*C*	*NC*	*NoCG or HG*
	C	$1,1$	$\in (0,1)^2$	
	NC	$\in (0,1)^2$	$0,0$	
$\tilde{\boldsymbol{\xi}}^*_C$		*C*	*NC*	*PD, NoCG or HG*
	C	$1,1$	$\in (-1,1)\times(0,2)$	
	NC	$\in (0,2)\times(-1,1)$	$0,0$	
$\tilde{\boldsymbol{\xi}}^*_{NC}$		*C*	*NC*	*PD, NoCG or HG*
	C	$1,1$	$\in (-1,1)\times(0,2)$	
	NC	$\in (0,2)\times(-1,1)$	$0,0$	

We focus on the first three endemic steady states, which are the most relevant. To understand what happens at the steady states from a strategic point of view, we start by considering frameworks with exogenous ruling quantities in (9), namely those in which $i_t - \theta_t$ is constant. If $i_t = \theta_t$, the corresponding payoff matrix is the one reported in the middle column of the first row. In such case, any coupling between C and NC strategies is a Nash equilibrium. This means that, in a framework without coevolution between the epidemiological situation, the perceived thresh-

old of alert, and the strategic interaction, multiple Nash equilibria arise. It can also be shown that every mixed strategy coupling is a Nash equilibrium.

When coevolutionary mechanisms are introduced, the conditions under which a steady state is characterized by $i^* = \theta^* = i_R$ require a specific distribution of strategies among agents, namely the one for which the contact rate is $\frac{\gamma}{1-i_R}$, which is feasible only when $\omega^* = \omega_R^*$. We can therefore say that the coevolutionary mechanism selects a unique mixed-strategy Nash equilibrium in which strategy C (respectively, NC) is chosen with probability ω_R^* (respectively, $1 - \omega_R^*$).

Conversely, at the steady states $\boldsymbol{\xi}_C^*$ and $\boldsymbol{\xi}_{NC}^*$, the resulting games correspond, respectively, to a no-conflict/harmony game (whose Nash equilibrium is $(1, 1)$) and to a prisoner's dilemma (whose Nash equilibrium is $(0, 0)$). In both cases, the steady state features a homogeneous population (of cooperating agents in the former, and of non-cooperating ones in the latter). The two steady states can thus be identified with two pure-strategy Nash equilibria.

We note that $\boldsymbol{\xi}_C^*$ is feasible when $\gamma < (1 - i_R)\alpha_C$. In such a scenario, the perceived level of alert is always so high (namely, the perceived threshold above which the epidemiological situation is considered risky is so low) that even if the entire population adopted the control measures implemented by the regulator, it would not be possible to achieve $i^* = i_R$. In this case, the situation drives agents to adopt containment measures more and more widely, which evolutionarily leads to the selection of a configuration characterized by cooperation.

At $\boldsymbol{\xi}_{NC}^*$, the opposite occurs. Since this steady state is feasible only when $\gamma > (1 - i_R)\alpha_{NC}$, the perceived level of alert is so low that even without the adoption of any measure by all agents we would have $i^* < i_R$. Hence, a homogeneous non-cooperating behavior yields a higher average payoff than any other distribution of strategies.

Contrasting Propositions 3 and 4, we observe that at the disease-free steady states only the prisoner's dilemma game emerges, while at the endemic steady states all three possible kinds of games compatible with the expression for $\mathcal{T}$ and $\mathcal{S}$ in (9), i.e., the prisoner's dilemma, the no-conflict game and the harmony game, can emerge.

In particular, as remarked above, at some of the endemic steady states, different games can arise according to the parameter values. For instance, at $\boldsymbol{\xi}_C^*$ both the no-conflict game, characterized by $0 < \mathcal{S} < \mathcal{T} < 1$, and the harmony game, with $0 < \mathcal{T} < \mathcal{S} < 1$, can emerge. According to the proof of Proposition 4, in the Appendix, at $\boldsymbol{\xi}_C^*$ we have $\mathcal{T} = 1 - \tau\left(1 - \frac{\gamma}{\alpha_C}\right)$ and $\mathcal{S} = -\sigma\left(1 - \frac{\gamma}{\alpha_C}\right)$. Hence, $\mathcal{T} > \mathcal{S}$ for $1 > (\tau - \sigma)\left(1 - \frac{\gamma}{\alpha_C}\right)$ or, equivalently, for $\tau - \sigma < \frac{1}{1-\frac{\gamma}{\alpha_C}}$, i.e., when the reactivity parameters are small enough in absolute value, and thus the total strategic reactivity is sufficiently low. Indeed, we recall that both the no-conflict game and the harmony game are characterized by a loss associated with defection. However, in the no-conflict game, such a loss is smaller than in the harmony game, due to the reduced relevance given to the strategic interaction in the former, so the incentive toward cooperation is lower in the no-conflict game than in the harmony game. Regarding the threshold value $\frac{1}{1-\frac{\gamma}{\alpha_C}}$ for the total strategic reactivity, we stress that it coincides with the inverse of $i_C := 1 - \frac{\gamma}{\alpha_C}$, i.e., of the best endemic state, that emerges when $\omega = 1$, i.e., when the population is composed solely of cooperating agents. With an increase in i_C, the threshold for the total strategic reactivity $\tau - \sigma$ to pass from a no-conflict game to a harmony game falls, as a worse epidemic situation stimulates cooperation.

Similarly, it is possible to explain the occurrence of the same two games at $\left(1 - \frac{\gamma}{\alpha_{NC}}, 0, 0\right)$, where $\mathcal{T} > \mathcal{S}$ occurs for $\tau - \sigma < \frac{1}{1-\frac{\gamma}{\alpha_{NC}}}$. Note that, symmetrically with what occurs at $\boldsymbol{\xi}_C^*$, it holds that $i_{NC} := 1 - \frac{\gamma}{\alpha_{NC}}$ is the worst endemic state, which emerges when $\omega = 0$, i.e., when the population is composed solely of defecting agents.

Focusing instead on $\tilde{\boldsymbol{\xi}}_C^*$ and $\tilde{\boldsymbol{\xi}}_{NC}^*$, in addition to the no-conflict game and the harmony game, also the prisoner's dilemma game, characterized by $\mathcal{S} < 0 < 1 < \mathcal{T}$, can emerge, when the epidemic situation is perceived as particularly safe. Namely, considering for instance $\tilde{\boldsymbol{\xi}}_C^*$, according

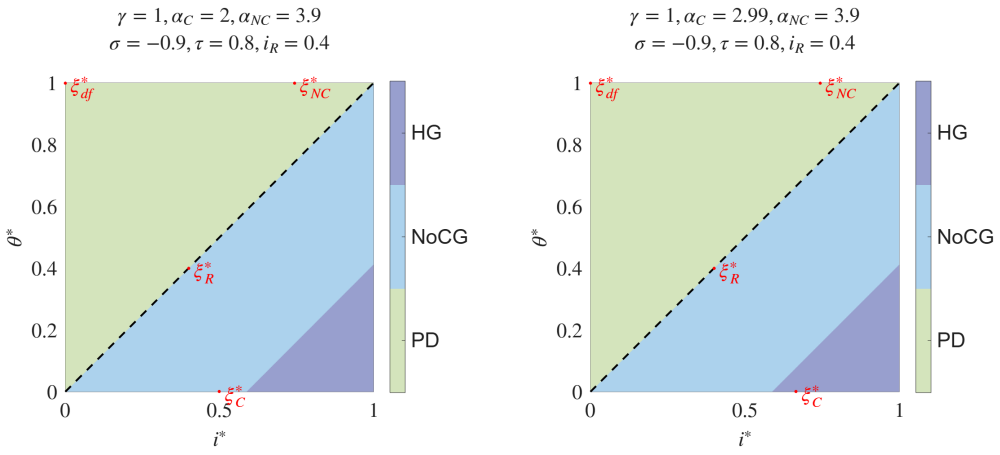

Figure 2: For different parameter configurations, possible steady state games. PD stands for prisoner's dilemma, NoCG for no-conflict game and HG for harmony game.

to the proof of Proposition 4, it holds that $\mathcal{T} = 1 - \tau\left(1 - \frac{\gamma}{\alpha_C} - \theta\right)$ and $\mathcal{S} = -\sigma\left(1 - \frac{\gamma}{\alpha_C} - \theta\right)$. Thus, $\mathcal{T}$ can exceed 1, and symmetrically $\mathcal{S}$ can become negative, for high values of the alert threshold θ.

Two possible steady state configurations, resulting from different choices of the parameters that determine their existence and position, are shown in the plane of the possible equilibrium values of i and θ in Figure 2.

3.2 Dynamical analysis

We start focusing on the stability of $\boldsymbol{\xi}^*_C$ and $\boldsymbol{\xi}^*_{NC}$.

Proposition 5. *Steady state* $\boldsymbol{\xi}^*_C = \left(1 - \frac{\gamma}{\alpha_C}, 0, 1\right)$*, which exists for* $\gamma < (1 - i_R)\alpha_C$*, is locally asymptotically stable for* $\gamma > \alpha_C - 2$*, while steady state* $\boldsymbol{\xi}^*_{NC} = \left(1 - \frac{\gamma}{\alpha_{NC}}, 1, 0\right)$*, which exists for* $(1 - i_R)\alpha_{NC} < \gamma < \alpha_{NC}$*, is locally asymptotically stable for* $\gamma > \alpha_{NC} - 2$*.*

The stability condition for $\boldsymbol{\xi}^*_C$ (respectively, $\boldsymbol{\xi}^*_{NC}$) coincides with that of the endemic steady state of an SIS model with the corresponding contact rate α_C (respectively, α_{NC}). For both $\boldsymbol{\xi}^*_C$ and $\boldsymbol{\xi}^*_{NC}$, neither the mechanism determining the perceived alert threshold, nor the responsiveness of the strategy payoffs, nor their evolutionary selection has any effect on stability.

Proposition 6. *Both steady states* $\left(1 - \frac{\gamma}{\alpha_C}, 1, 1\right)$, $\left(1 - \frac{\gamma}{\alpha_{NC}}, 0, 0\right)$*, when they exist, and* $(0, 1, 1)$ *are always unstable.*

The steady states considered in Proposition 6 cannot be stable. From the interpretative point of view, this is quite predictable. Let us consider for example $\left(1 - \frac{\gamma}{\alpha_C}, 1, 1\right)$. In such case, the steady state population is homogeneous, and composed just by cooperating agents, even if the steady perceived alert threshold, above which the epidemic situation is considered risky by agents, is the highest possible, since $\theta^* = 1$, meaning that agents believe that the health situation is completely under control. This is a consequence of the evolutionary selection process based on a replicator-type mechanism: its imitative nature, in the presence of a homogeneous population, leads to its preservation. However, any small perturbation in the population distribution that

causes some agents to become non-cooperative, under conditions of null alert, gains an evolutionary advantage and therefore tends to spread further, moving away from the initial steady-state condition.

Proposition 7. *Steady state $\boldsymbol{\xi}^*_{df} = (0, 1, 0)$ is locally asymptotically stable for $\gamma > \alpha_{NC}$.*

The stability condition of the unique possibly stable disease-free steady state coincides with that of the disease-free steady state in the classic SIS model, with the recovery rate that must be sufficiently high relative to the maximal possible contact rate. In this case the epidemic trajectory can converge toward disease eradication, and, once it has been eradicated from the population, further transmission is no longer possible, except in the presence of exogenous perturbations that reintroduce the pathogen.

The next stability result deals with the continua of endemic equilibria $\tilde{\boldsymbol{\xi}}^*_C$ and $\tilde{\boldsymbol{\xi}}^*_{NC}$. In these situations, the analysis of the Jacobian matrix is not always sufficient, since for certain parameter configurations the two steady states are not hyperbolic. We do not pursue a deeper stability analysis here, but we simply specify the parameter settings for which $\tilde{\boldsymbol{\xi}}^*_C$ and $\tilde{\boldsymbol{\xi}}^*_{NC}$ are hyperbolic; in such cases, they are unstable.

Proposition 8. *Steady state $\tilde{\boldsymbol{\xi}}^*_C = (i_R, \theta, 1)$, when it exists, is unstable if $\gamma < \alpha_C - 2$ or if $\theta > 1 - \frac{\gamma}{\alpha_C}$. Steady state $\tilde{\boldsymbol{\xi}}^*_{NC} = (i_R, \theta, 0)$, when it exists, is unstable if $\gamma < \alpha_{NC} - 2$ or if $\theta < 1 - \frac{\gamma}{\alpha_{NC}}$.*

We note that under the condition $\gamma < \alpha_C - 2$, both steady states $\boldsymbol{\xi}^*_C$ and $\tilde{\boldsymbol{\xi}}^*_C$ are unstable, and a similar situation occurs for $\boldsymbol{\xi}^*_{NC}$ and $\tilde{\boldsymbol{\xi}}^*_{NC}$ when $\gamma < \alpha_{NC} - 2$. Moreover, recalling the comments on Proposition 6, we emphasize that when the steady state consists of a homogeneous population with a perceived alert level that is strongly inconsistent with the strategy adopted by the population, the steady state is unstable.

In the last stability results, we focus on $\boldsymbol{\xi}^*_R$. In more detail, in Proposition 9 we will emphasize the effect of ρ, while in Proposition 10 we will let the role of β emerge.

In view of the stability analysis of $\boldsymbol{\xi}^*_R$ with respect to ρ, let us introduce the threshold values

$$\tilde{\beta} := \frac{\beta\, i_R(1 - i_R)A}{(\alpha_{NC} - \alpha_C)^2} > 0, \tag{17}$$

where

$$A := \left(\alpha_{NC} - \frac{\gamma}{1 - i_R}\right)\left(\frac{\gamma}{1 - i_R} - \alpha_C\right)\left[\tau\left(\alpha_{NC} - \frac{\gamma}{1 - i_R}\right) - \sigma\left(\frac{\gamma}{1 - i_R} - \alpha_C\right)\right], \tag{18}$$

$$\tilde{\rho}_{ns,j} := 1 - \frac{1 + \frac{\gamma i_R}{1 - i_R} \pm \sqrt{\left(1 + \frac{\gamma i_R}{1 - i_R}\right)^2 - 4\tilde{\beta}}}{2\tilde{\beta}},\ j = 1,\, 2, \tag{19}$$

where $\tilde{\rho}_{ns,1}$ and $\tilde{\rho}_{ns,2}$ correspond to the above expression with "+" and "−" signs, respectively,

$$\tilde{\rho}_{fl} := 2\left(1 - \frac{2}{\tilde{\beta}}\left(\frac{\gamma i_R}{1 - i_R} - 2\right)\right), \tag{20}$$

$$\beta_0 := \frac{\gamma(\alpha_{NC} - \alpha_C)^2}{(1 - i_R)^2 A} \tag{21}$$

and

$$\beta_\delta := \frac{\left(1 + \frac{\gamma i_R}{1 - i_R}\right)^2 (\alpha_{NC} - \alpha_C)^2}{4 i_R (1 - i_R) A},$$

in which we stress that subscripts $_{ns,j}$ and $_{fl}$ identify values at which a Neimark-Sacker bifurcation or a flip bifurcation are respectively possible.

Proposition 9. *Let $\gamma \leq 1$. Steady state $\boldsymbol{\xi}_R^*$, when it exists for $\alpha_C < \frac{\gamma}{1-i_R} < \alpha_{NC}$, is locally asymptotically stable if*

1. $\rho \in \left(0, \dfrac{\tilde{\rho}_{ns,2}}{4\sqrt{i_R\left(1-\sqrt{i_R}\right)}}\right)$ *for:*
   $i_R \in \left(0, \frac{2}{3}\right]$, $\beta < \beta_0$;
   $i_R \in \left(0, \frac{2}{3}\right]$, $\beta = \beta_0$, $\gamma > \frac{1-i_R}{i_R}$;
   $i_R \in \left(\frac{2}{3}, 1\right)$, $\beta < \beta_0$, $\gamma \leq \frac{2(1-i_R)}{i_R}$;
   $i_R \in \left(\frac{2}{3}, 1\right)$, $\beta = \beta_0$, $\frac{1-i_R}{i_R} < \gamma \leq \frac{2(1-i_R)}{i_R}$
2. $\rho \in \left(\dfrac{\tilde{\rho}_{ns,1}}{4\sqrt{i_R\left(1-\sqrt{i_R}\right)}}, \dfrac{\tilde{\rho}_{ns,2}}{4\sqrt{i_R\left(1-\sqrt{i_R}\right)}}\right)$ *for:*
   $i_R \in \left(\frac{1}{2}, \frac{2}{3}\right]$, $\beta \in (\beta_0, \beta_\delta)$, $\gamma \in \left(\frac{1-i_R}{i_R}, 1\right]$;
   $i_R \in \left(\frac{2}{3}, 1\right)$, $\beta \in (\beta_0, \beta_\delta)$, $\gamma \in \left(\frac{1-i_R}{i_R}, \frac{2(1-i_R)}{i_R}\right]$
3. $\rho \in \left(0, \dfrac{\min\{\tilde{\rho}_{ns,2}, \tilde{\rho}_{fl}\}}{4\sqrt{i_R\left(1-\sqrt{i_R}\right)}}\right)$ *for* $i_R \in \left(\frac{2}{3}, 1\right)$, $\beta \leq \beta_0$, $\gamma > \frac{2(1-i_R)}{i_R}$
4. $\rho \in \left(\dfrac{\tilde{\rho}_{ns,1}}{4\sqrt{i_R\left(1-\sqrt{i_R}\right)}}, \dfrac{\min\{\tilde{\rho}_{ns,2}, \tilde{\rho}_{fl}\}}{4\sqrt{i_R\left(1-\sqrt{i_R}\right)}}\right)$ *for:*
   $i_R \in \left(\frac{2}{3}, \frac{3+\sqrt{8}}{4+\sqrt{8}}\right]$, $\beta \in (\beta_0, \beta_\delta)$, $\gamma > \frac{2(1-i_R)}{i_R}$;
   $i_R \in \left(\frac{3+\sqrt{8}}{4+\sqrt{8}}, 1\right)$, $\beta \in (\beta_0, \beta_\delta)$, $\gamma \in \left(\frac{2(1-i_R)}{i_R}, \frac{(3+\sqrt{8})(1-i_R)}{i_R}\right]$

A first outcome of Proposition 9 is predictable: a strong perceived alert threshold reactivity parameter ρ induces instability. This occurs in all four possible cases and can take the form of either a flip or a Neimark-Sacker bifurcation. Such finding aligns with standard intuition, as an overly reactive adaptive threshold mechanism introduces oscillatory instabilities into the system.

More interestingly, ρ can also have a stabilizing effect, leading to the scenarios corresponding to Cases 2 and 4. In these two situations, $\boldsymbol{\xi}_R^*$ is stable within an intermediate range $\rho \in$ (lower bound, upper bound), while becoming unstable for both exceedingly low and high values of ρ. For this scenario to arise, an intermediate level of evolutionary pressure (β) is required and, more importantly, the recovery rate (γ) must be sufficiently high. In Figure 3, we depict the region of the (i_R, γ)-plane for which the pairing of i_R and γ satisfies the conditions specified in Cases 2 and 4.[6] Within the union of these regions, certain parameter combinations lead to unfeasible (empty) constraints (indicated in white), once it is taken into account that $\boldsymbol{\xi}_R^*$ exists only if $\alpha_{NC} > \frac{\gamma}{1-i_R}$, and that, according to (16), the positivity of the model trajectories requires

[6] For Case 2, the lower and upper bounds correspond, respectively, to the dashed red and black curves, whereas for Case 4, the lower and upper bounds correspond, respectively, to the dashed black and blue curves.

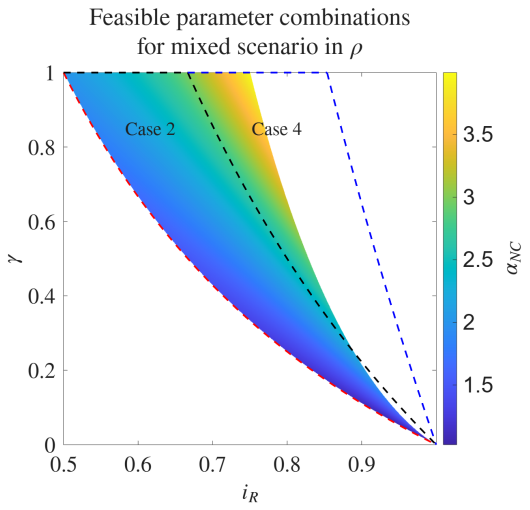

Figure 3: Region of the (i_R, γ)-plane for which the pairing of i_R and γ satisfies the conditions specified in Cases 2 and 4 of Proposition 9. Parameter couplings that provide empty constraints are depicted in white, while blue to yellow colors identify the minimum feasible value of α_{NC}.

$\alpha_{NC} < (1 + \sqrt{\gamma})^2$. The color scale encodes the minimum value of α_{NC} for which there exist combinations of parameters satisfying the conditions[7] associated with Cases 2 and 4.

When the recovery rate is high and the regulator accepts a high target i_R, the adaptive threshold mechanism acts as a stabilizing feedback strictly within a specific reactivity range. If ρ is too low, the perception of risk is sluggish, allowing infections to accumulate before triggering a delayed, over-compensatory behavioral shift. Conversely, the evolutionary dynamics - by maintaining a mixed population ($\omega^* \in (0, 1)$) - provides additional selection pressure that constrains θ and prevents complete polarization, enabling this stabilizing effect at intermediate ρ.

We remark that the instability at high ρ can occur via two distinct bifurcation mechanisms, revealing different *endogenous origins* of the instability. In particular, the flip bifurcation is primarily associated with endogenous epidemiological instability.
Conversely, a Neimark-Sacker bifurcation generates quasi-periodic oscillations emerging from an endogenous dynamical instability. This arises from the interaction and mutual delay among the system's constituent domains, propagating along the following three-way feedback cycle:

$$\text{High } i_t \xrightarrow{\text{alert thr.}} \text{Low } \theta_t \xrightarrow{\text{evolut.}} \text{High } \omega_t \xrightarrow{\text{epidem.}} \text{Low } i_t \xrightarrow{\text{alert thr.}}$$

$$\text{High } \theta_t \xrightarrow{\text{evolut.}} \text{Low } \omega_t \xrightarrow{\text{epidem.}} \text{High } i_t$$

The Neimark-Sacker bifurcation thus accounts for a socio-epidemiological-evolutionary instability involving all three model components. When ρ is too high, the adaptive mechanism becomes overly sensitive, locking the variables into an oscillatory joint mode.

A deeper and somewhat counterintuitive insight can emerge in scenarios characterized by high transmission rates α_C and α_{NC}. Under such conditions, the discrete-time SIS epidemiological subsystem becomes intrinsically unstable on its own, primarily driven by large infection overshoots that mathematically manifest as flip bifurcations. This epidemiological instability dominates the extremes of the feasible i_R range. Here, the high force of infection triggers violent oscillations that cannot be tamed. However, for intermediate values of the target incidence i_R,

[7]We stress that numerical investigations suggest that each feasible coupling of γ and i_R resulting from Figure 3 provides a non-empty interval for β and ρ for every σ, τ and for all admissible values of α_{NC} and α_C.

the coevolutionary framework allows for a window of stability. In such regime, the evolutionary dynamics and the adaptive perceived alert threshold do not merely perturb the system, but actually behave as an essential stability recovering mechanism by counteracting the discrete-time epidemiological overshoots. This stabilizing effect is based on a delicately tuned reactivity ρ and appropriate evolutionary pressure β. If ρ is too low or not supported by a suitable evolutionary pressure, risk perception adapts too slowly. The behavioral response fails to promptly brake the high transmission rates, allowing the intrinsic epidemiological volatility to bleed into the system and generate Neimark-Sacker quasi-periodic oscillations. Ultimately, the interplay between strong evolutionary pressure (β) and moderate reactivity (ρ) is shown to be capable of overriding structural epidemiological instabilities, provided that the regulator targets an intermediate endemic state.

The analysis of the role played by β on the stability of $\boldsymbol{\xi}_R^*$ is deepen in the next result. To such aim, recalling (18), we introduce

$$\hat{\rho} := \frac{\gamma i_R}{1 - i_R + \gamma i_R}, \tag{22}$$

$$\hat{\gamma} := \frac{\rho(1 - i_R)\tilde{\imath}_R}{i_R(1 - \rho\tilde{\imath}_R)(2\rho\tilde{\imath}_R - 1)}, \tag{23}$$

$$\beta_{fl} := \frac{4\left(\frac{\gamma i_R}{1-i_R} - 2\right)(\alpha_{NC} - \alpha_C)^2}{i_R(1 - i_R)(2 - \rho\tilde{\imath}_R)A} \tag{24}$$

and

$$\beta_{ns} := \frac{\left[\gamma i_R - \rho\tilde{\imath}_R(\gamma i_R + 1 - i_R)\right](\alpha_{NC} - \alpha_C)^2}{i_R(1 - i_R)^2(1 - \rho\tilde{\imath}_R)^2 A}, \tag{25}$$

where

$$\tilde{\imath}_R := 4\sqrt{i_R\left(1 - \sqrt{i_R}\right)}. \tag{26}$$

We remark that also the subscripts associated with the thresholds in (24) and (25) indicate, respectively, the occurrence of possible flip and Neimark-Sacker bifurcations.

Proposition 10. *Steady state* $\boldsymbol{\xi}_R^* = \left(i_R, i_R, \frac{\alpha_{NC} - \frac{\gamma}{1-i_R}}{\alpha_{NC} - \alpha_C}\right)$, *when it exists for* $\alpha_C < \frac{\gamma}{1-i_R} < \alpha_{NC}$, *is locally asymptotically stable if*

- $\beta \in (0, \beta_{ns})$ *for:*

  $i_R \in \left(0, \frac{2}{3}\right]$, $\rho \leq \frac{1}{8\sqrt{i_R\left(1-\sqrt{i_R}\right)}}$, $\rho < \frac{\hat{\rho}}{4\sqrt{i_R\left(1-\sqrt{i_R}\right)}}$;

  $i_R \in \left(0, \frac{2}{3}\right]$, $\frac{1}{8\sqrt{i_R\left(1-\sqrt{i_R}\right)}} < \rho < \frac{\hat{\rho}}{4\sqrt{i_R\left(1-\sqrt{i_R}\right)}}$, $\frac{1-i_R}{i_R} < \gamma \leq \min\{1, \hat{\gamma}\}$;

  $i_R \in \left(\frac{2}{3}, 1\right)$, $\rho < \frac{\hat{\rho}}{4\sqrt{i_R\left(1-\sqrt{i_R}\right)}}$, $\gamma \leq \frac{2(1-i_R)}{i_R}$

- $\beta \in (\beta_{fl}, \beta_{ns})$ *for:*

  $i_R \in \left(\frac{2}{3}, 1\right)$, $\rho \leq \frac{1}{8\sqrt{i_R\left(1-\sqrt{i_R}\right)}}$, $\rho < \frac{\hat{\rho}}{4\sqrt{i_R\left(1-\sqrt{i_R}\right)}}$, $\frac{2(1-i_R)}{i_R} < \gamma \leq 1$;

  $i_R \in \left(\frac{2}{3}, 1\right)$, $\frac{1}{8\sqrt{i_R\left(1-\sqrt{i_R}\right)}} < \rho < \frac{\hat{\rho}}{4\sqrt{i_R\left(1-\sqrt{i_R}\right)}}$, $\frac{2(1-i_R)}{i_R} < \gamma \leq \min\{1, \hat{\gamma}\}$

Contrasting Propositions 9 and 10, we note that, similarly to what occurs with ρ, also on increasing β two different outcomes can arise. In addition to the predictable one, according to which a strong evolutionary pressure induces instability, we find that β can also have a stabilizing effect, i.e., $\boldsymbol{\xi}_R^*$ is stable for β assuming intermediate values, when the reaction of the adaptive threshold mechanism is not excessive and the recovery rate is large enough. However, differently from Proposition 9, the destabilization at high β can occur just via a Neimark-Sacker bifurcation, giving rise to quasi-periodic oscillations, while the stabilization on raising β occurs via a flip bifurcation. The rationale underlying this behavior can be developed via arguments similar to those previously carried out for ρ.[8]

Some insights on comparative dynamics, in particular in regard to possible convergence towards different steady states on raising i_R, will be presented together with the simulative analysis in Section 4.

4 Simulative analysis

In this section, we present numerical investigations to further explore the role of some parameters - particularly i_R - and to study the possible dynamics away from equilibrium. In particular, simulations are performed by choosing $\sigma = -0.9$ and $\gamma = 1$ and considering either $\tau = 0.1$ or $\tau = 0.8$, which outline situations in which $\mathcal{T}_t$ depends only weakly or, respectively, strongly on $i_t - \theta_t$, and which are thus, in turn, associated, respectively, with pronounced asymmetry or substantial symmetry between the reaction coefficients τ and σ. Moreover, the case of $\tau = 0.8$ and $\sigma = -0.9$ allows us to consider a situation in which the strategic interaction exhibits a sensitive dependence on the endogenous components.

The choice of γ instead corresponds to the maximum possible value in the SIS model. In this regard, recall that in the classic SIS model, with an exogenous contact rate α, the endemic steady state is stable for $\gamma < \alpha < \gamma + 2$, with the behavior as α varies described by the bifurcation diagram shown in Figure 4. In particular, when $\gamma = 1$, if $\alpha < 1$ the unique steady state is the disease-free one, which incurs a transcritical bifurcation at $\alpha = 1$ and is replaced by the stable endemic steady state for $1 < \alpha < 3$. At $\alpha = 3$ the disease-free steady state becomes unstable through a flip bifurcation, and convergence is toward a periodic or chaotic endemic attractor, depending on α. High values of γ are the most dynamically interesting, as they encompass the greatest variety of possible scenarios as α varies (see condition (16)). In what follows, we consider three different frameworks that, with reference to homogeneous populations entirely composed of cooperators or non-cooperators, differ in terms of the stability properties of the classic SIS model. More precisely, by "stable/unstable α_i" we refer to the values of α_i for which the SIS model with contact rate α_i (corresponding to a homogeneous population of agents $i \in \{C, NC\}$) admits an endemic equilibrium that is locally asymptotically stable/unstable.

To summarize the scenarios arising from Proposition 9, we represent in Figures 5–10 and 12–15 the stability regions in the (i_R, ρ)-plane. Colors denote parameter combinations for which either all stability conditions of the endemic equilibrium are satisfied (white), only the stability condition associated with a possible Neimark-Sacker (respectively, flip) bifurcation is violated (green and, respectively, magenta), or more than one stability condition is violated (blue). Transitions from white to colored regions therefore indicate a loss of stability, while transitions from colored to white regions indicate stability recovery. The nature of the possible bifurcations can be inferred from the color of the instability regions and will be further investigated through one-dimensional bifurcation diagrams. Note that transitions between green/magenta and blue regions, and vice versa, do not correspond to bifurcations. In what follows, the black bifurcation diagrams are obtained from initial conditions chosen sufficiently close to the endemic equilibria, whereas

[8] We stress that, since $\hat{\gamma}$ depends on ρ, an illustration analogous to Figure 3 would exhibit an explicit dependence on the parameter ρ. For this reason, we refrain from providing a corresponding graphical representation for Proposition 10.

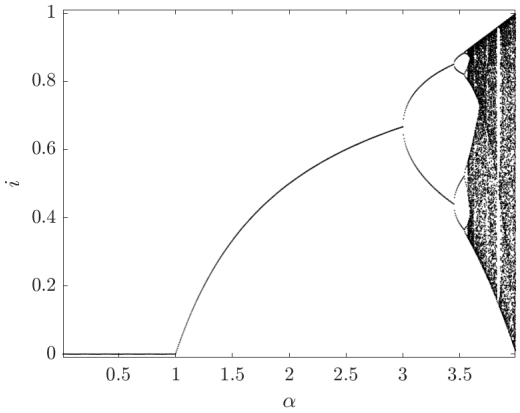

Figure 4: Bifurcation diagram for i as α increases in the classic SIS model, for $\gamma = 1$.

the initial conditions used for the red diagrams are specified explicitly for each simulation.
The combinations of parameters for which the only existing endemic equilibrium is $\boldsymbol{\xi}_R^*$ are those lying between the two vertical dotted lines $i_R = 1 - \frac{\gamma}{\alpha_C}$ and $i_R = 1 - \frac{\gamma}{\alpha_{NC}}$. To the left of $i_R = 1 - \frac{\gamma}{\alpha_C}$ (respectively, to the right of $i_R = 1 - \frac{\gamma}{\alpha_{NC}}$), the only existing endemic equilibrium is $\boldsymbol{\xi}_C^*$ (respectively, $\boldsymbol{\xi}_{NC}^*$). Finally, we consider values of i_R over intervals slightly larger than $\left(1 - \frac{\gamma}{\alpha_C}, 1 - \frac{\gamma}{\alpha_{NC}}\right)$, since the stability of $\boldsymbol{\xi}_C^*$ and $\boldsymbol{\xi}_{NC}^*$ does not depend on i_R, whenever they exist.

4.1 Both stable α_C and α_{NC}

We consider $\alpha_C = 1.2$ and $\alpha_{NC} = 2.9$. In this framework, steady state $\boldsymbol{\xi}_R^*$ exists for $i_R \in (0.167, 0.656)$, and endemic equilibria $\boldsymbol{\xi}_C^*$ and $\boldsymbol{\xi}_{NC}^*$ are stable respectively for $i_R < 0.167$ and $i_R > 0.626$. We performed numerical investigations for $i_R \in (0.1, 0.72)$ and $\rho \in (0, 0.8)$.

We start considering $\tau = 0.1$, for which the related simulations are reported in Figure 5. We begin by analyzing the role of i_R, which can be inferred from horizontal cross-sections of the stability regions. The main observation is that sufficiently large values of ρ can induce instability even in parameter regimes in which the epidemiological subsystem alone would remain stable. Moreover, this destabilizing effect becomes stronger as β increases, since the stability region of $\boldsymbol{\xi}_R^*$ progressively shrinks, indicating that, within this framework, the evolutionary pressure is always destabilizing.
In further detail, for sufficiently small values of β (Panels (a)–(c)), $\boldsymbol{\xi}_R^*$ is stable for all i_R provided that ρ is small. The bifurcation diagram corresponding to (a) is shown in Panel (e). As ρ increases, $\boldsymbol{\xi}_R^*$ becomes unstable for $i_R \in \left(1 - \frac{\gamma}{\alpha_C}, \rho_{ns,2}\right)$, and it may recover stability through a reverse Neimark-Sacker bifurcation on growing i_R (see Panel (f), stabilizing scenario). If ρ is further increased, the threshold value of i_R above which $\boldsymbol{\xi}_R^*$ is stable also raises, until $\boldsymbol{\xi}_R^*$ becomes unstable for all $i_R \in \left(1 - \frac{\gamma}{\alpha_C}, 1 - \frac{\gamma}{\alpha_{NC}}\right)$.
If we consider larger values of β, a slight increase in ρ from the value at which the destabilizing scenario arises leads to a further increase in complexity. In this case, $\boldsymbol{\xi}_R^*$, after initially recovering stability, subsequently loses it and then recovers it again as i_R increases, giving rise to a stabilizing-destabilizing-stabilizing scenario, as shown in the bifurcation diagram reported in Panel (g). If β is further increased (Panel (c)), as ρ grows there first appears a scenario characterized by Neimark-Sacker bubbling (a destabilizing-stabilizing scenario), described by the bifurcation diagram in Panel (g), which is then followed, as ρ is further increased, by the stabilizing-destabilizing-stabilizing, the stabilizing, and in the end the fully unstable scenarios. Finally, if β

is very large (Panel (d)), the bubbling destabilizing-stabilizing scenario occurs even for arbitrarily small values of ρ.

We now turn to the analysis of the role of ρ, which can be inferred from vertical cross-sections of the stability regions. In this case, ρ always acts as a destabilizing factor when i_R is close to either $1 - \frac{\gamma}{\alpha_C}$ or $1 - \frac{\gamma}{\alpha_{NC}}$ (see the bifurcation diagram in Panel (i)), with instability thresholds that may display a non-monotonic dependence on i_R. However, for intermediate values of i_R and sufficiently large β, $\boldsymbol{\xi}_R^*$ may be unstable for all values of ρ, or it may exhibit an initial instability for small ρ that is subsequently recovered, so that $\boldsymbol{\xi}_R^*$ becomes stable over a limited range of ρ values, before finally losing stability again as ρ increases (see Panel (j)).

We emphasize that numerical simulations indicate that, for larger values of α_C, no new qualitative scenarios emerge: the sequence of scenarios remains essentially unchanged and depends on τ, although raising α_C larger values of β are required to trigger transitions between different sequences. In other words, the scenarios become less sensitive to evolutionary pressure when increasing α_C. Moreover, the stability regions tend to grow as α_C approaches α_{NC}, with the stability of $\boldsymbol{\xi}_R^*$ being preserved for larger values of ρ.

In addition to these identified scenarios, Panel (j) reveals the occurrence of multistability, with a chaotic attractor (in red, obtained setting $i_0 = 0.8\, i_R$, $\theta_0 = 0.8\, i_R$ and $\omega_0 = 0.8\, \omega_R^*$) firstly coexisting with $\boldsymbol{\xi}_R^*$ and then with the quasi-periodic attractor arising from its stability loss. In Figure 6 we report the corresponding basins of attraction as ρ increases. Yellow areas indicate the basins of attraction of $\boldsymbol{\xi}_R^*$ (in Panels (a)–(c), black asterisk) and of the quasi-periodic attractor (in Panels (d)–(f), black dots), whereas blue areas denote the basins of the chaotic attractor (Panels (a)–(f), red dots). Note that the yellow regions shrink as ρ increases, until the quasi-periodic attractor collides with the boundary of the basin and subsequently disappears.

Now we set $\tau = 0.8$ and we report the results of the simulations in Figure 7. For the stability regions (Panels (a)–(d)), the conclusions drawn for the case $\tau = 0.1$ remain largely applicable. We highlight only a few differences. First, one can observe a modest reduction in potential complexity due to the disappearance of the stabilizing–destabilizing–stabilizing scenario. Moreover, the results show an increased sensitivity to β: due to the higher reactivity $\tau = 0.8$, the stability region of $\boldsymbol{\xi}_R^*$ shrinks faster and for smaller values of β. Since the bifurcation diagrams for the different scenarios remain qualitatively the same as those reported in the case of $\tau = 0.1$, we avoid to report them, while we focus on possible time series arising when $\boldsymbol{\xi}_R^*$ is unstable, which may be qualitatively quite different according to the values of i_R. We have both long time periods of low infection levels interrupted by quick upsurges/downturns of infections (Panel (e)) and irregular (Panel (f)) or smooth (Panel (g)) quasi-periodic behaviors. We emphasize that this descriptive variety of quasi-periodic dynamics is not restricted to this specific parameter set; rather, an in-depth simulation analysis has shown that it regularly occurs.

In Panels (h)-(i) we show the possible long-run strategic interactions. In Panel (h), all three endemic equilibria $\boldsymbol{\xi}_C^*$ (blue), $\boldsymbol{\xi}_R^*$ (red) and $\boldsymbol{\xi}_{NC}^*$ (black) are stable and the associated strategic outcomes are, respectively, the no-conflict game, an indifferent scenario with a mixed-strategy equilibrium, and the prisoner's dilemma, as shown in Panel (h).

When $\boldsymbol{\xi}_R^*$ is unstable (Panel (i)), the dynamics approach an attractor in which strategic interactions alternate between no-conflict game and the prisoner's dilemma. A similar behavior is observed when $\tau = 0.1$, with the only difference being that the reduced reactivity in this case does not allow for the emergence of a harmony game, which could in principle arise when $\tau = 0.8$, even though it does not occur in the simulation reported in Panel (i).

Finally, we examine whether system trajectories can converge to $\tilde{\boldsymbol{\xi}}_C^*$ and $\tilde{\boldsymbol{\xi}}_{NC}^*$. Recall that these equilibria form continua of steady states, arising only for a specific value of i_R each (given by $1 - \frac{\gamma}{\alpha_C}$ and $1 - \frac{\gamma}{\alpha_{NC}}$) at which the system undergoes a transition from $\boldsymbol{\xi}_C^*$ to $\boldsymbol{\xi}_R^*$ and from $\boldsymbol{\xi}_R^*$ to $\boldsymbol{\xi}_{NC}^*$, respectively. Proposition 8 established the conditions on parameter θ under which the continua $\tilde{\boldsymbol{\xi}}_C^*$ and $\tilde{\boldsymbol{\xi}}_{NC}^*$ are unstable. The outcomes of the numerical simulations are reported in

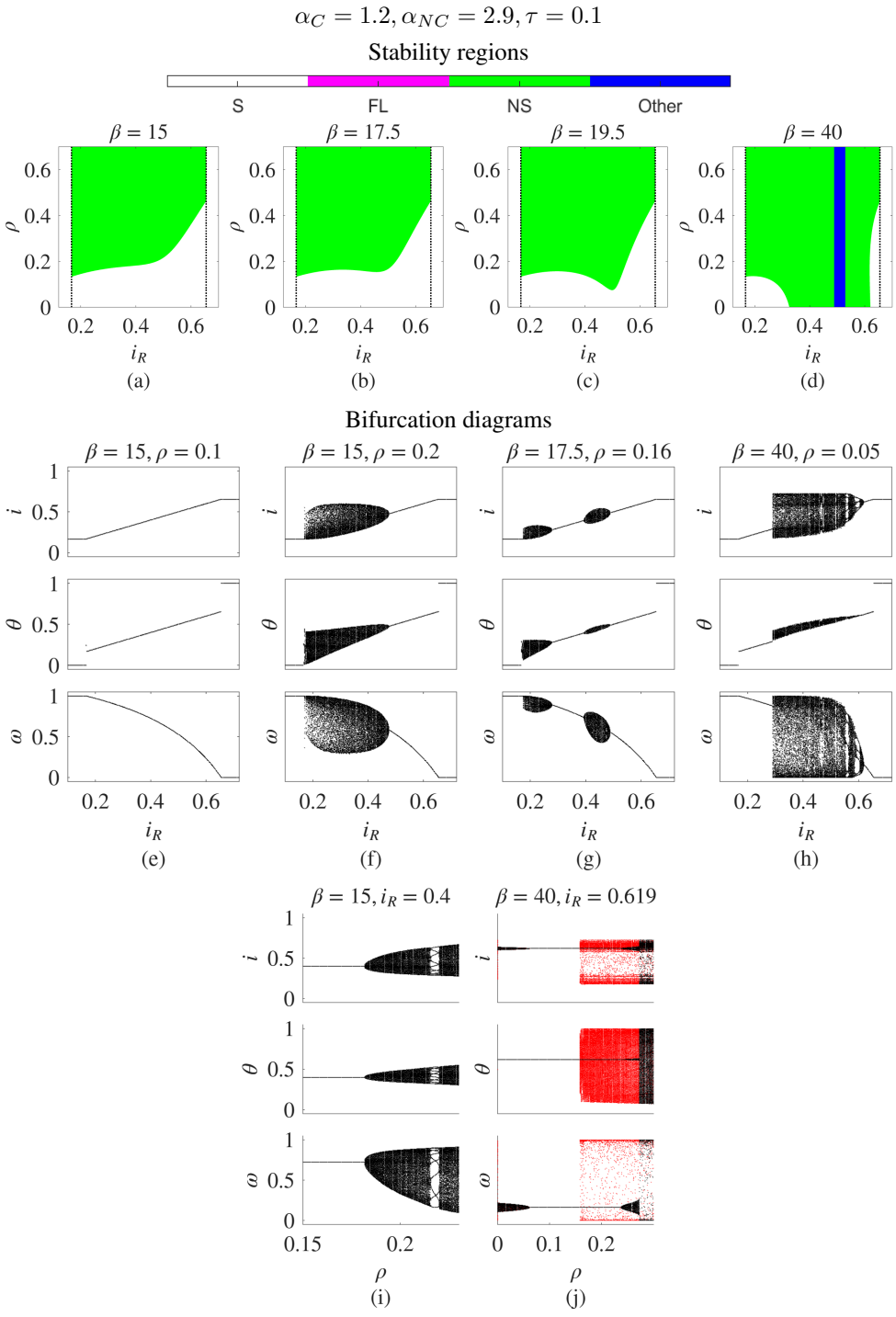

Figure 5: Case of both stable endemic steady states of homogeneous populations of cooperators and non-cooperators ($\alpha_C = 1.2$ and $\alpha_{NC} = 2.9$) and low reactivity $\tau = 0.1$. Panels (a)–(d): stability regions for different values of β. Panels (e)–(h): bifurcation diagrams on increasing i_R. Panels (i)-(j): bifurcation diagrams on increasing ρ, with (j) showing coexistence between different kinds of attractors.

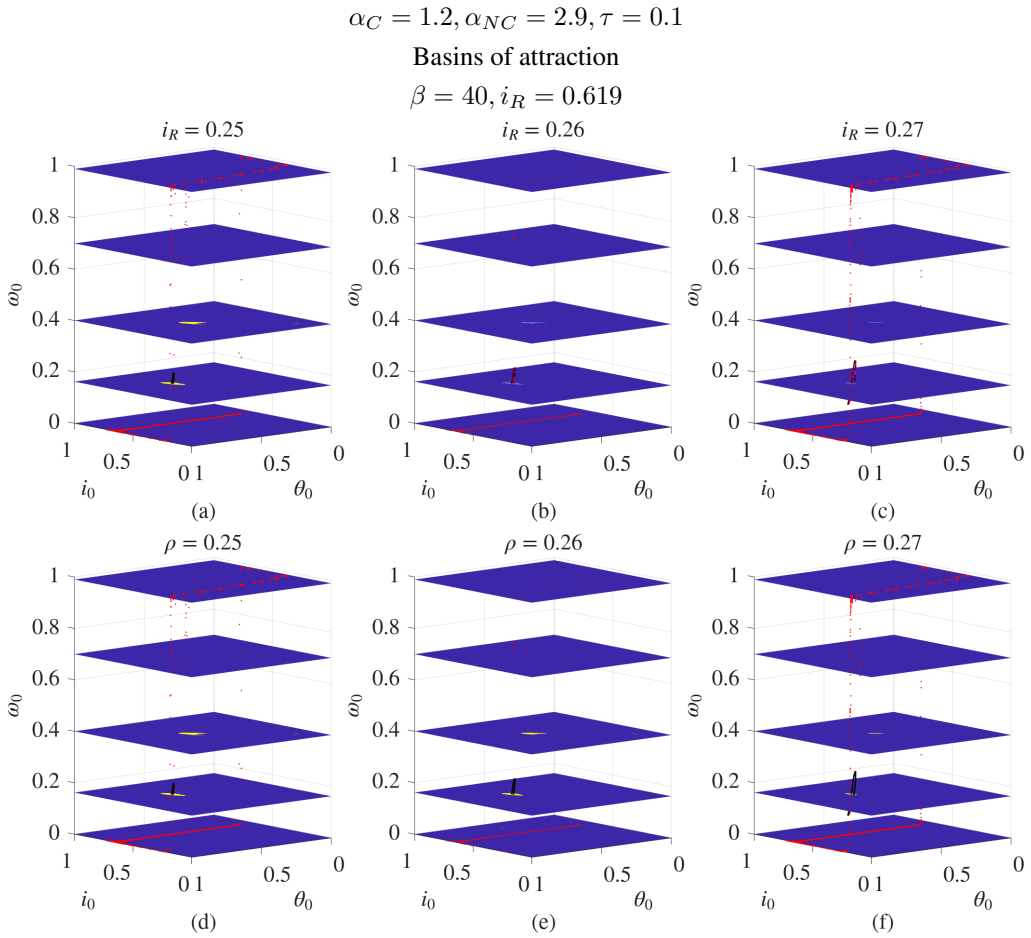

Figure 6: Case of both stable endemic steady states of homogeneous populations of cooperators and non-cooperators ($\alpha_C = 1.2$ and $\alpha_{NC} = 2.9$) and low reactivity $\tau = 0.1$, and for $\beta = 40$, $i_R = 0.619$. Panels (a)–(c): basins of attraction for different values of i_R showing coexistence between $\boldsymbol{\xi}_R^*$ and a chaotic attractor. Panels (d)–(f): basins of attraction for different values of ρ showing coexistence between a quasi-periodic and a chaotic attractors.

Figures 8 and 9, corresponding to $\tau = 0.1$ and $\tau = 0.8$, respectively.
In the two figures, Panels (a) display cross-sections of the basins of attraction for selected values of the initial condition ω_0. These sections reveal the presence of infinitely many attractors of the form $\left(1 - \frac{\gamma}{\alpha_{NC}}, \theta, 0\right)$, represented by the blue-to-yellow color gradient associated with $\theta \in \left(1 - \frac{\gamma}{\alpha_{NC}}, 1\right)$. Although the geometry of the basins varies with the values of the parameters, all numerical simulations consistently indicate that the continuum of steady states $\tilde{\boldsymbol{\xi}}_{NC}^*$ is stable for any $\theta \in \left(1 - \frac{\gamma}{\alpha_{NC}}, 1\right)$, regardless of the values of β and ρ.
Panels (b) in Figures 8 and 9 illustrate, in the (i, θ, ω) space, the continuum of steady states attained by the system (black line), together with several representative trajectories (dashed lines) converging to different points on it. The red plane corresponds to $\theta = 1 - \frac{\gamma}{\alpha_{NC}}$, which defines the lower boundary of the stable subset of steady states $\tilde{\boldsymbol{\xi}}_{NC}^*$. Similar conclusions apply to the continuum of steady states $\tilde{\boldsymbol{\xi}}_C^*$.
Panels (c) in Figures 8 and 9 reveal the presence of infinitely many attractors of the form $\left(1 -\right.$

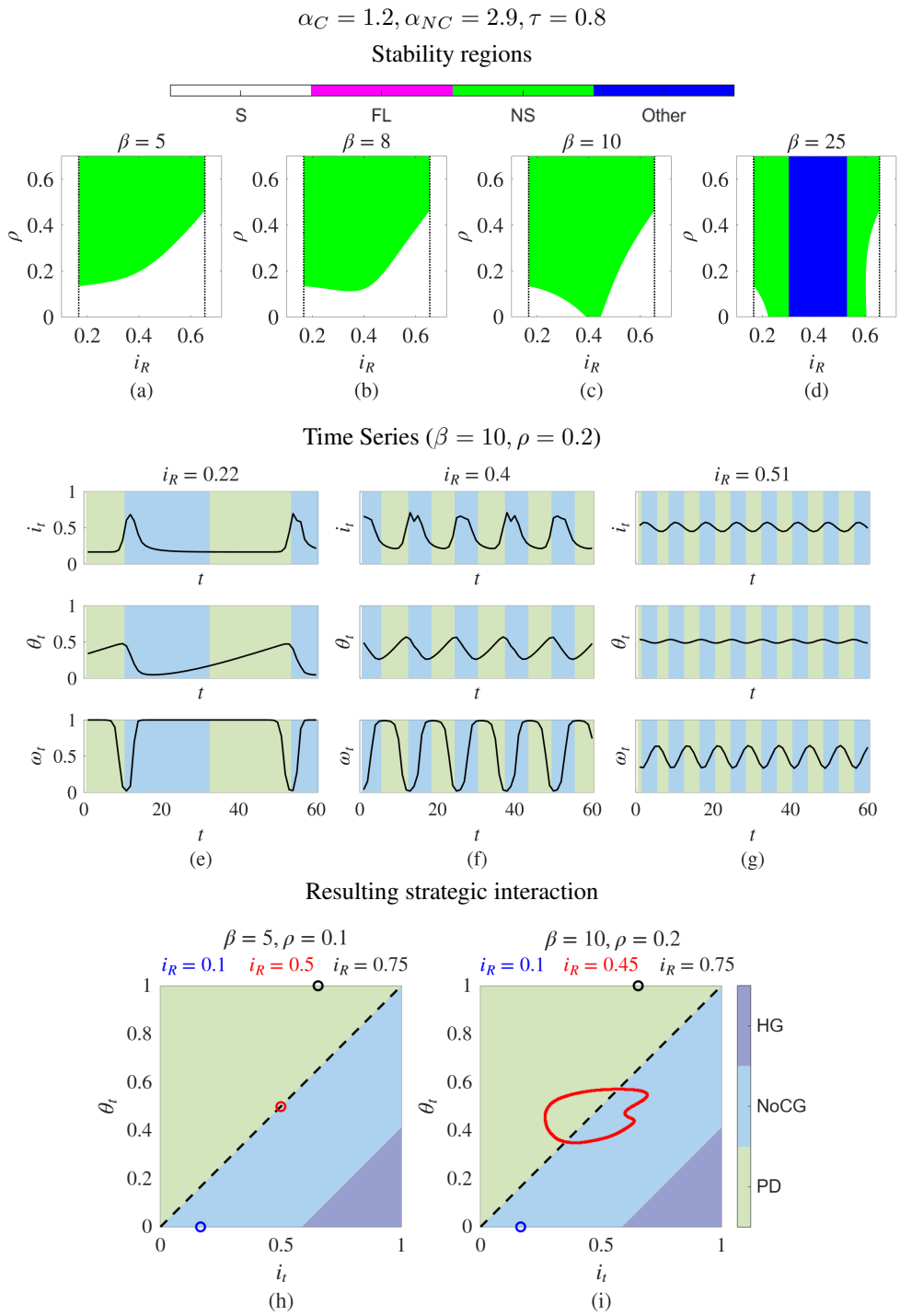

Figure 7: Case of both stable endemic steady states of homogeneous populations of cooperators and non-cooperators ($\alpha_C = 1.2$ and $\alpha_{NC} = 2.9$) and large reactivity $\tau = 0.8$. Panels (a)–(d): stability regions for different values of β. Panels (e)–(g): quasi-periodic trajectories for different values of i_R. Panels (h)-(i): resulting games for different values of β, ρ and i_R.

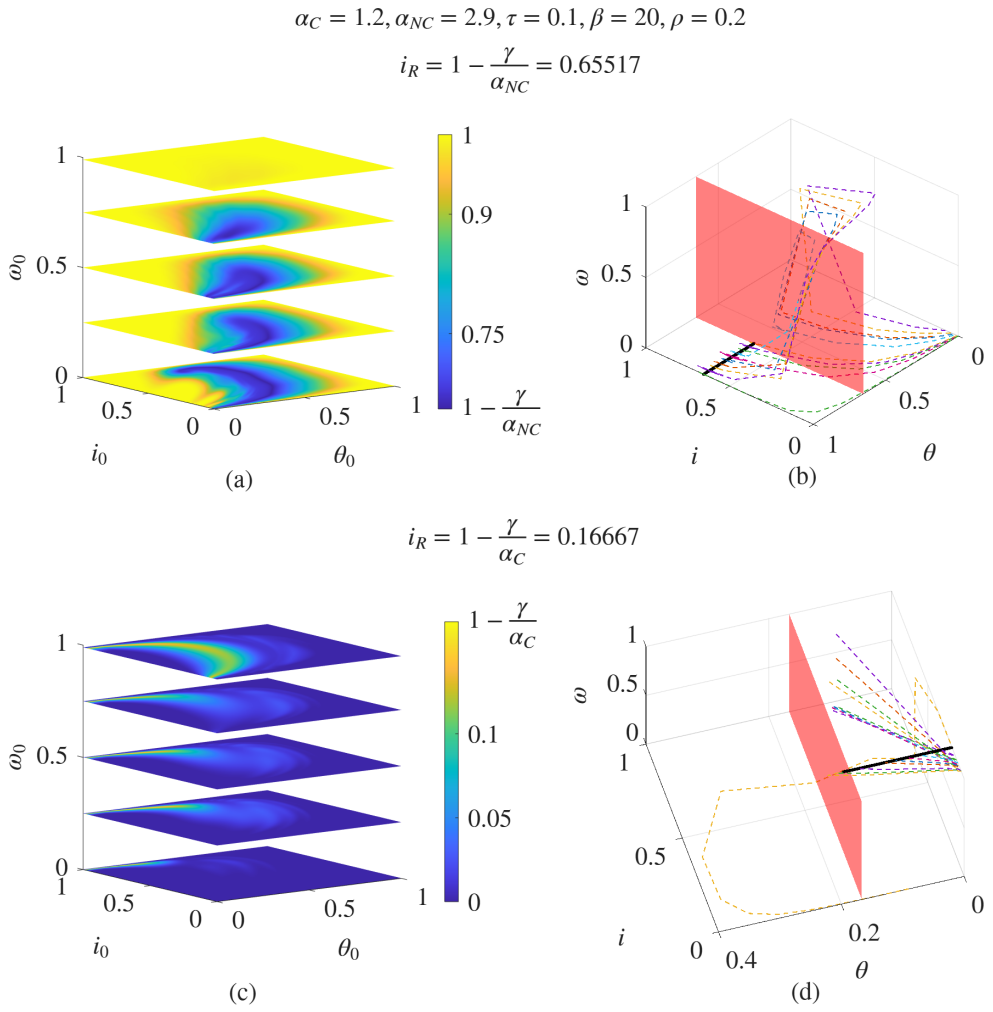

Figure 8: Basins of attraction of the continuum $\tilde{\boldsymbol{\xi}}^*_{NC}$ when $i_R = 1 - \frac{\gamma}{\alpha_{NC}}$ (Panel (a)) and of the continuum $\tilde{\boldsymbol{\xi}}^*_{C}$ when $i_R = 1 - \frac{\gamma}{\alpha_C}$ (Panel (c)), for $\tau = 0.1$, $\beta = 20$ and $\rho = 0.2$. Different steady states are represented by distinct colors, referring to the corresponding colorbar. The continua of stable steady states $\tilde{\boldsymbol{\xi}}^*_{NC}$ (Panel (b)) and $\tilde{\boldsymbol{\xi}}^*_{C}$ (Panel (d)) are represented by the black line, together with trajectories converging toward some of them (dashed lines). Red planes delimit the values of θ for which $\tilde{\boldsymbol{\xi}}^*_{NC}$ and $\tilde{\boldsymbol{\xi}}^*_{C}$ are stable.

$\frac{\gamma}{\alpha_C}, \theta, 1\big)$, represented by the blue-to-yellow color gradient associated with $\theta \in \big(0, 1 - \frac{\gamma}{\alpha_C}\big)$. Each color shade identifies a distinct attractor within the continuum.

As in the previous case, in both figures, Panels (d) depict the continuum of steady states attained by the system (black line), together with several representative trajectories (dashed lines) converging to different points on it. The red plane corresponds to $\theta = 1 - \frac{\gamma}{\alpha_C}$ and marks the upper boundary of the stable branch of steady states $\tilde{\boldsymbol{\xi}}^*_{C}$.

Similar conclusions hold for steady states $\tilde{\boldsymbol{\xi}}^*_{C}$ considered in the frameworks analyzed in the following subsections for stable α_C. In contrast, whenever the contact rate α_i, for $i = C$ or $i = NC$, satisfies the instability conditions of Proposition 8, we find no numerical evidence of attractors lying on the continuum $\tilde{\boldsymbol{\xi}}^*_{i}$. In such cases, the trajectories instead converge to the attractors indicated in red.

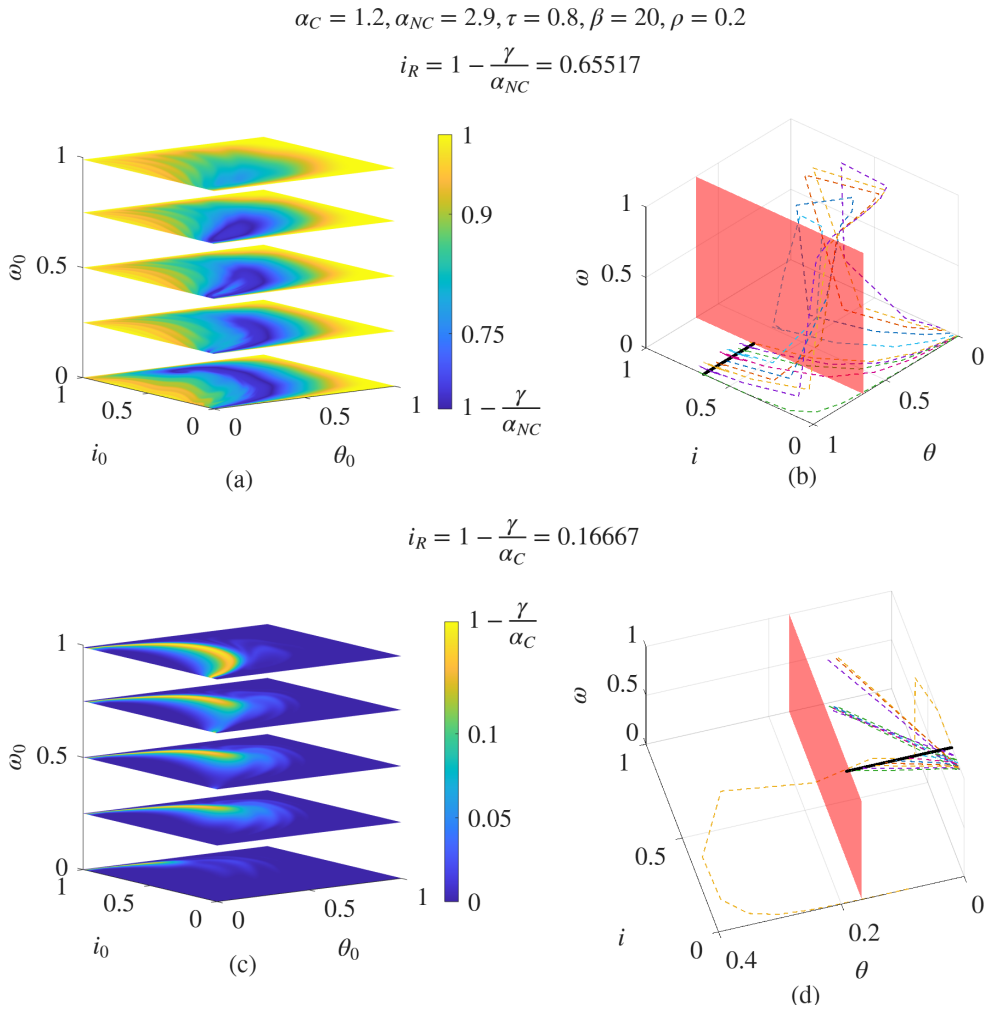

Figure 9: Basins of attraction of the continuum $\tilde{\boldsymbol{\xi}}^*_{NC}$ when $i_R = 1 - \frac{\gamma}{\alpha_{NC}}$ (Panel (a)) and of the continuum $\tilde{\boldsymbol{\xi}}^*_{C}$ when $i_R = 1 - \frac{\gamma}{\alpha_C}$ (Panel (c)), for $\tau = 0.8$, $\beta = 20$ and $\rho = 0.2$. Different steady states are represented by distinct colors, referring to the corresponding colorbar. The continua of stable steady states $\tilde{\boldsymbol{\xi}}^*_{NC}$ (Panel (b)) and $\tilde{\boldsymbol{\xi}}^*_{C}$ (Panel (d)) are represented by the black line, together with trajectories converging toward some of them (dashed lines). Red planes delimit the values of θ for which $\tilde{\boldsymbol{\xi}}^*_{NC}$ and $\tilde{\boldsymbol{\xi}}^*_{C}$ are stable.

4.2 Stable α_C and unstable α_{NC}

We deal with two cases, both characterized by $\alpha_{NC} = 3.9$. We note that for such contact rate, the isolated SIS model exhibits chaotic dynamics. In the present model, endemic equilibrium $\boldsymbol{\xi}^*_{NC}$ then exists for $i_R > 0.744$, and is unstable.

In the first case we set $\alpha_C = 1.2$, so steady state $\boldsymbol{\xi}^*_R$ exists for $i_R \in (0.167, 0.754)$, while the endemic equilibrium $\boldsymbol{\xi}^*_C$ exists and is stable for $i_R < 0.167$. Results are reported for $i_R \in (0.12, 0.78)$ and $\rho \in (0, 0.8)$.

We start by considering $\tau = 0.1$, and we make reference to Figure 10 for the discussion. Looking at the stability regions reported in Panels (a)–(d) we can highlight two main differences with those in Figures 5 and 7. Firstly, $\boldsymbol{\xi}^*_R$ can become unstable through a flip bifurcation. This can occur both as i_R and ρ increase when moving from white to magenta regions

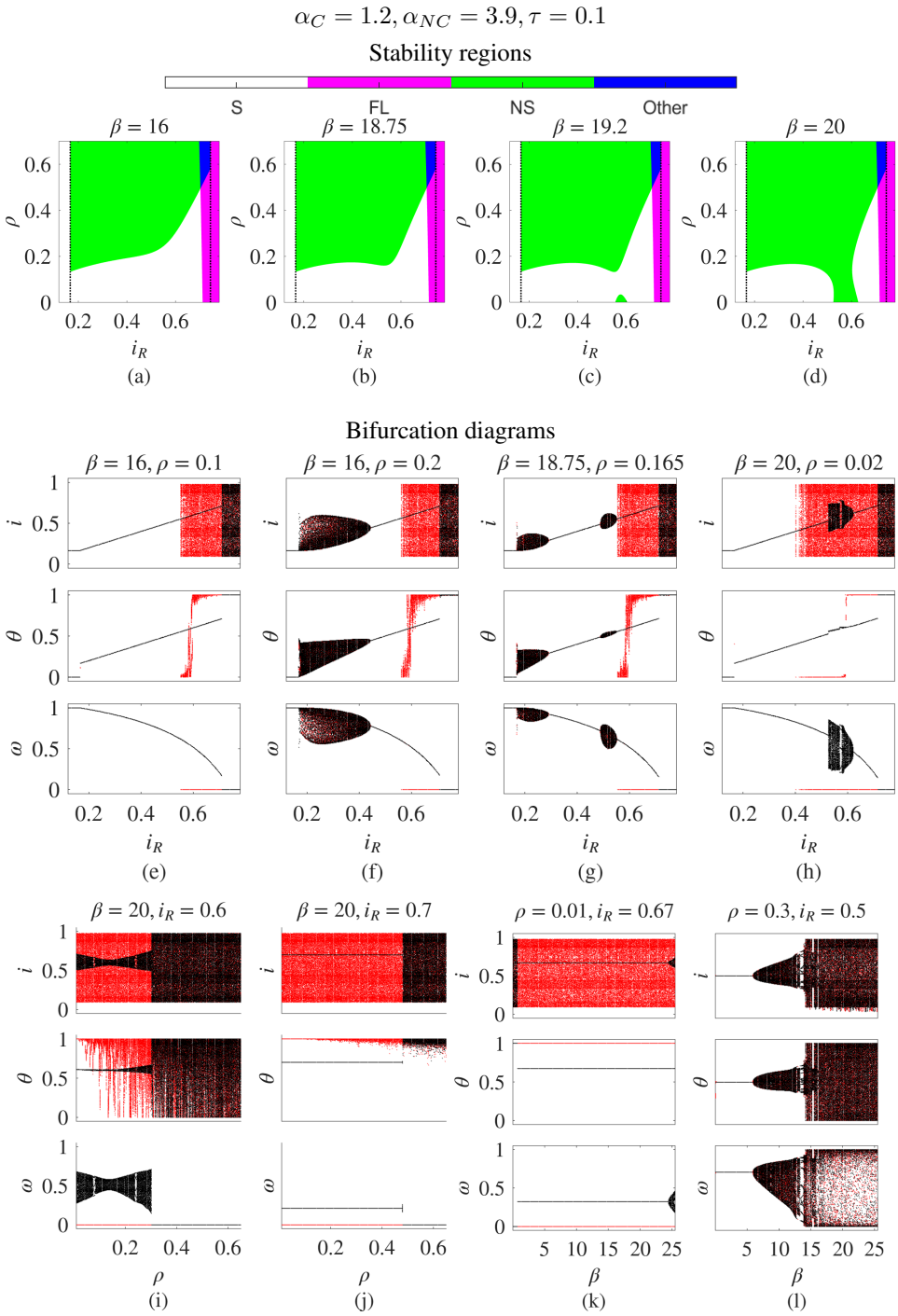

Figure 10: Case of stable endemic steady state for homogeneous cooperators and unstable one for homogeneous non-cooperators ($\alpha_C = 1.2$ and $\alpha_{NC} = 3.9$), with low reactivity $\tau = 0.1$. Panels (a)–(d): stability regions for different values of β. Panels (e)–(h): bifurcation diagrams on increasing i_R. Panels (i)-(j): bifurcation diagrams on increasing ρ. Panels (k)-(l): bifurcation diagrams on increasing β. In Panels (e)–(l) red and black colors refer to different initial data.

(crossing curve $\rho = \rho_{fl}$). As a consequence, each scenario identified by stability changes as i_R increases in the case of both α_C and α_{NC} being stable is now replaced, when α_C is stable and α_{NC} is unstable, by a new scenario exhibiting the same sequence of stability changes, but with an additional final destabilization induced by a flip bifurcation. The actual occurrence of such scenarios is highlighted in the bifurcation diagrams in black and red (these latter generated setting $i_0 = 0.8\, i_R$, $\theta_0 = 1 - 10^{-8}$ and $\omega_0 = 10^{-8}$), obtained as i_R increases, in Panels (e)–(h). The resulting bifurcation scenarios for $\boldsymbol{\xi}_R^*$ are the flip destabilizing scenario (Panel (e)), the NS stabilizing-flip destabilizing scenario (Panel (f)), the NS stabilizing-NS destabilizing-NS stabilizing-flip destabilizing scenario (Panel (g)) and the NS destabilizing-NS stabilizing-flip destabilizing scenario (Panel (h)), where NS stands for Neimark-Sacker. The black bifurcation diagram in Panel (j) shows the new flip destabilizing scenario occurring on increasing ρ. The bifurcation diagrams in Panel (i) report a case where $\boldsymbol{\xi}_R^*$ is unstable for all values of ρ. Finally, the bifurcation diagrams in Panels (k) and (l) show the two possible scenarios for $\boldsymbol{\xi}_R^*$ on increasing β, i.e., in agreement with Proposition 10, the NS destabilizing scenario and (in black in Panel (k)) the flip stabilizing-NS destabilizing scenario. In Panels (i)–(l), the red bifurcation diagrams are generated using the initial conditions $i_0 = 0.8\, i_R$, $\theta_0 = 0.99$ and $\omega_0 = 0.01$. Moreover, Panel (c) shows that as ρ increases, a Neimark-Sacker bubbling can reduce and disappear, a behavior not observed in the simulations reported in Figures 5 and 7.

In Figure 11 we display the basins of attraction for different parameter values. Panels (a)–(c) correspond to $\beta = 16$ and $\rho = 0.2$, the same values used in the bifurcation diagrams of Figure 10 (f). As already seen in previous simulations, also this framework reveals the coexistence of multiple attractors, as shown in Panels (e)–(j). These diagrams indicate the presence, for certain values $i_R < 0.754$, of a chaotic attractor with $\omega = 0$ that remains stable. Numerical exploration further shows that, when $\boldsymbol{\xi}_{NC}^*$ loses stability (according to Proposition 5, at $\alpha_{NC} = \gamma + 2 = 3$), another attractor persists and stays stable even for $\gamma < (1 - i_R)\alpha_{NC}$. The difference between the coexistence shown in Figure 5 and that in the present framework is that in this latter situation the chaotic attractor is directly connected with the dynamics of the isolated SIS model, while in the former case it arose from the highly nonlinear interaction among the different spheres. Yellow areas indicate the basins of attraction of $\boldsymbol{\xi}_R^*$ (black asterisk), whereas blue areas denote the basins of the chaotic attractor (red dots). As in the example reported in Figure 6, the basin of attraction of $\boldsymbol{\xi}_R^*$ shrinks as i_R increases. When i_R reaches the threshold $\rho = \rho_{fl}$ and $\boldsymbol{\xi}_R^*$ undergoes a flip bifurcation, a period-two cycle emerges but almost immediately collides with the boundary of its basin and vanishes. This accounts for why only the chaotic attractor appears in red in Figures 10 (e)–(j), and why the period–two cycle emerging from the flip bifurcation of $\boldsymbol{\xi}_R^*$ is absent. Panels (d)–(f) in Figure 11 use the same parameters as in the bifurcation diagrams of Figure 10 (i), namely $\beta = 20$ and $i_R = 0.6$, which indicate the coexistence of a quasi-periodic and a chaotic attractor. Also in this case, the yellow regions, representing now the basins of the quasi-periodic black attractor, progressively shrink as ρ increases, until it collides with the blue region (the basin of the red chaotic attractor) and subsequently disappears.

In Figure 12, we set $\tau = 0.8$ while keeping $\alpha_C = 1.2$ and $\alpha_{NC} = 3.9$. The stability regions (Panels (a)–(d)) indicate that a larger τ qualitatively simplifies the behavior, as there is no longer evidence that increasing ρ causes first a contraction and finally the disappearance of the Neimark-Sacker bubble. Moreover, consistently with Figure 7, the case with three stability transitions via potential Neimark-Sacker bifurcations no longer occurs for large τ. In Panel (e) we show the flip destabilization on increasing ρ, in which the period-two cycle, just after arising, collides with the boundary of the basin of attraction and convergence occurs toward a coexisting chaotic attractor (the red bifurcation diagram is obtained starting from $i_0 = 0.8\, i_R$, $\theta_0 = 0.8\, i_R$ and $\omega_0 = 0.8\, \omega_R^*$). Panel (f) depicts the possible dynamics for $\beta = 1$ and $\rho = 0.7$, for various values of i_R. In this case, differently from Figure 7 (i) the red quasi-periodic attractor also passes through the region associated with the harmony game.

In Figure 13 we consider $\alpha_C = 2.5$, larger than in the former framework analyzed in this

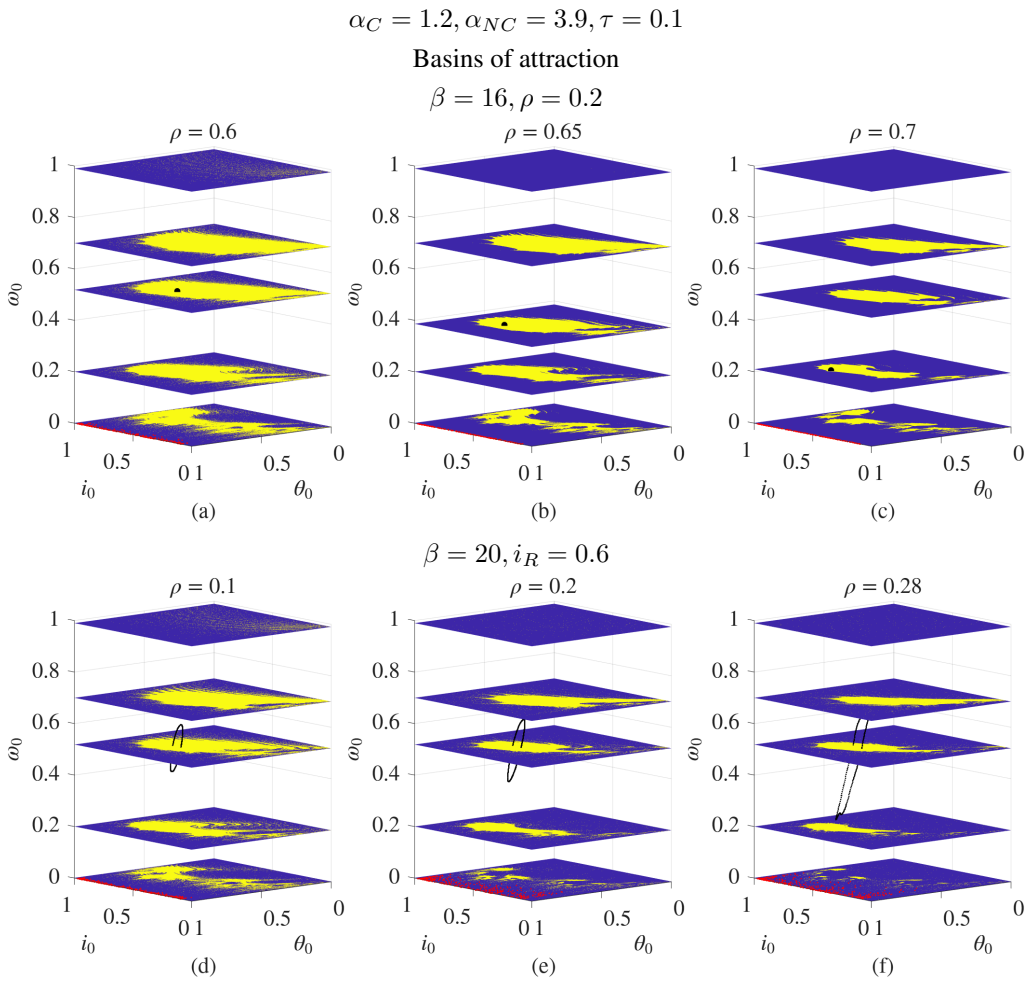

Figure 11: Case of stable endemic steady state for homogeneous cooperators and unstable one for homogeneous non-cooperators ($\alpha_C = 1.2$ and $\alpha_{NC} = 3.9$), with low reactivity $\tau = 0.1$. Panels (a)–(c): basins of attraction for $\beta = 16$, $\rho = 0.2$ and different values of i_R. Panels (d)–(f): basins of attraction for $\beta = 20$, $i_R = 0.6$ and different values of ρ.

subsection. Steady state $\boldsymbol{\xi}_R^*$ exists for $i_R \in (0.6, 0.754)$, while the endemic equilibrium $\boldsymbol{\xi}_C^*$ exists and is stable for $i_R < 0.6$. Results are reported for $i_R \in (0.57, 0.77)$ and $\rho \in (0, 0.8)$. As we can see, no additional scenarios arise; hence, bifurcation diagrams are omitted, as simulations indicate that they are qualitatively equivalent to those already shown in Figures 10 and 12. We only note a lower sensitivity to β, which must take larger and more variable values to trigger scenario changes.

For $\tau = 0.1$ (Panels (a)–(e)), the main difference from Figures 10 (a)–(d) is the altered sequence of scenarios on increasing i_R, for different fixed values of ρ. Namely, unlike in Figure 10, in Figure 13 the stabilizing-destabilizing-stabilizing-destabilizing scenario occurs before the emerge of the Neimark-Sacker bubble for low values of ρ. This is why in Figure 10 there is no analogue of Figure 13 (c).

In contrast, for $\tau = 0.8$ (Panels (f)–(i)), with respect to Figure 12 we can additionally observe the configuration in Panel (h), characterized by an instability region at small ρ that disappears at intermediate values. This configuration did not occur in the corresponding case with $\tau = 0.8$ and

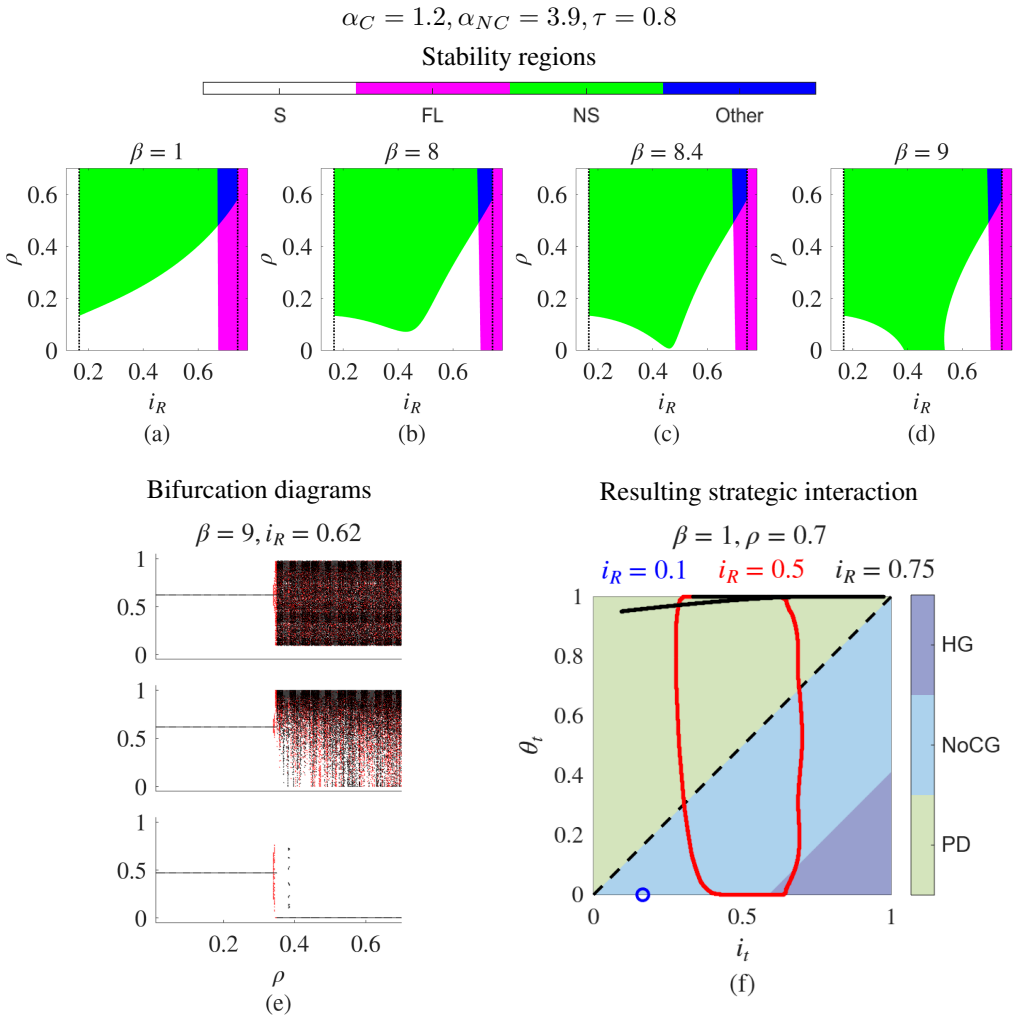

Figure 12: Case of stable endemic steady state for homogeneous cooperators and unstable one for homogeneous non-cooperators ($\alpha_C = 1.2$ and $\alpha_{NC} = 3.9$), with high reactivity $\tau = 0.8$. Panels (a)–(d): stability regions for different values of β. Panel (e): bifurcation diagram showing the flip destabilizing scenario for ρ. Panel (f): resulting game for different values of i_R.

$\alpha_C = 1.2$ (Figures 12 (a)–(d)) and had previously been seen only for smaller values of τ.

4.3 Both unstable α_C and α_{NC}

We set $\alpha_C = 3.2$ and $\alpha_{NC} = 3.9$. In the present framework, steady state $\boldsymbol{\xi}_R^*$ exists for $i_R \in (0.6875, 0.744)$, while the two endemic equilibria, $\boldsymbol{\xi}_C^*$ and $\boldsymbol{\xi}_{NC}^*$, exist but are unstable for $i_R < 0.6875$ and $i_R > 0.744$, respectively. Note that for $\alpha_C = 3.2$ the isolated SIS model displays a period-two cycle. Numerical simulations were performed for $i_R \in (0.66, 0.76)$ and $\rho \in (0, 0.8)$.

Figure 14 reports the simulations for $\tau = 0.1$. Similar to what occurs in the transition from the configuration where both $\alpha_i \in \{C, NC\}$ are stable to the one with unstable α_{NC}, making α_C unstable also generates an additional (initial) flip bifurcation, now occurring for i_R slightly larger than $1 - \frac{\gamma}{\alpha_C} = 0.6875$. However, the reduced stability range of values of i_R seems to prevent the possible emergence of scenarios in which three stability changes occur via Neimark-Sacker bifur-

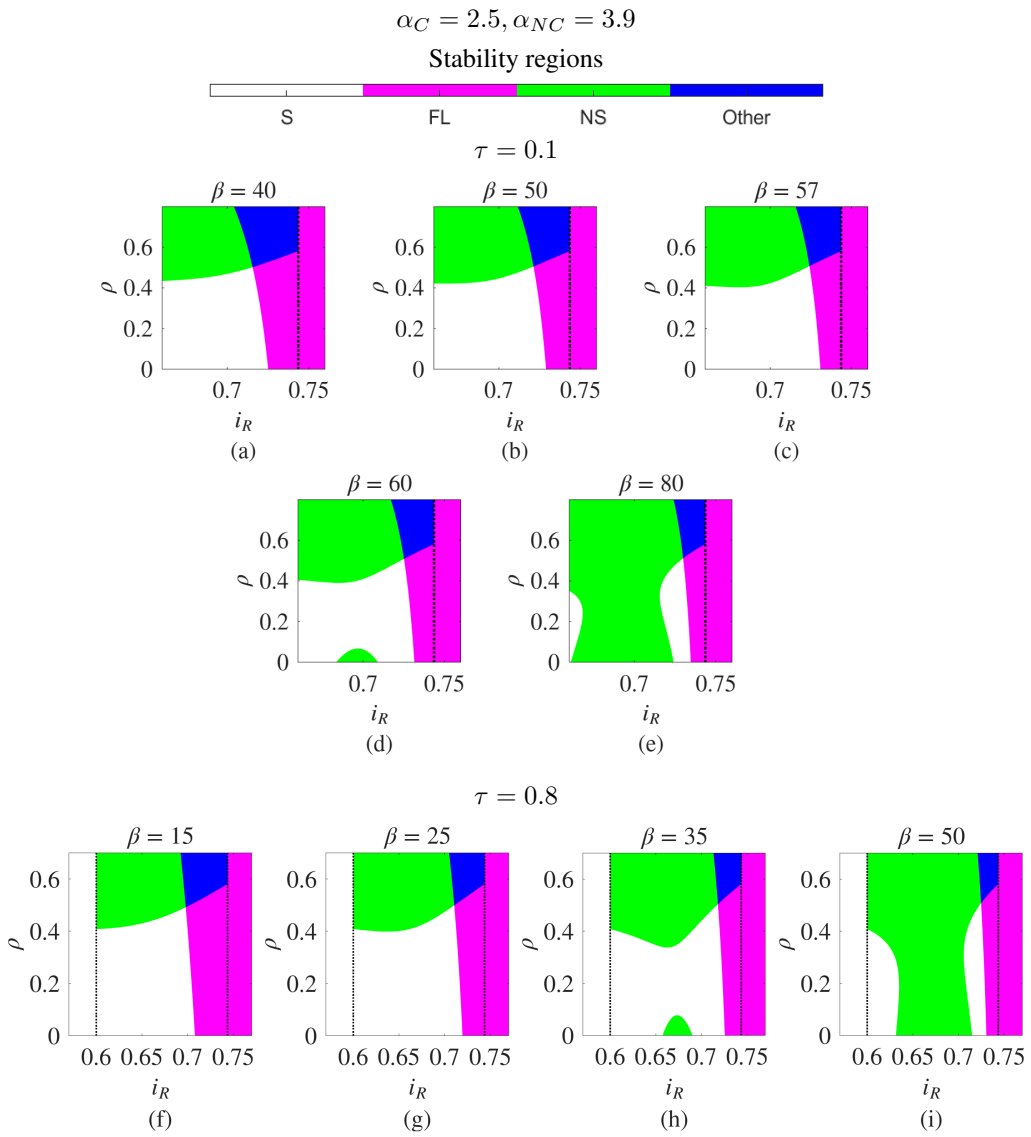

Figure 13: Case of stable endemic steady state for homogeneous cooperators and unstable one for homogeneous non-cooperators ($\alpha_C = 2.5$ and $\alpha_{NC} = 3.9$). Panels (a)–(e): stability regions for small reactivity $\tau = 0.1$, and for different values of β. Panels (f)–(i): stability regions for large reactivity $\tau = 0.8$, and for different values of β.

cations. Moreover, it is possible that each endemic state is unstable for any ρ and i_R, in particular for not sufficiently large values of β, as shown in Panel (a) and in the corresponding bifurcation diagrams in Panel (f). This outcome predictably aligns with the instability of endemic equilibria in homogeneous populations composed solely of cooperating or non-cooperating agents. However, driven by evolutionary selection and the adaptive mechanism that regulates the perception of the population of the alert threshold, a suitably chosen policy can restore the local stability of the endemic equilibrium $\boldsymbol{\xi}^*_R$, as indicated by the white areas in the stability regions in Panels (b)–(e) and the corresponding bifurcation plots in Panels (g)-(h). We stress that the coexistence between different attractors is present in this context, too, also characterized by various degrees

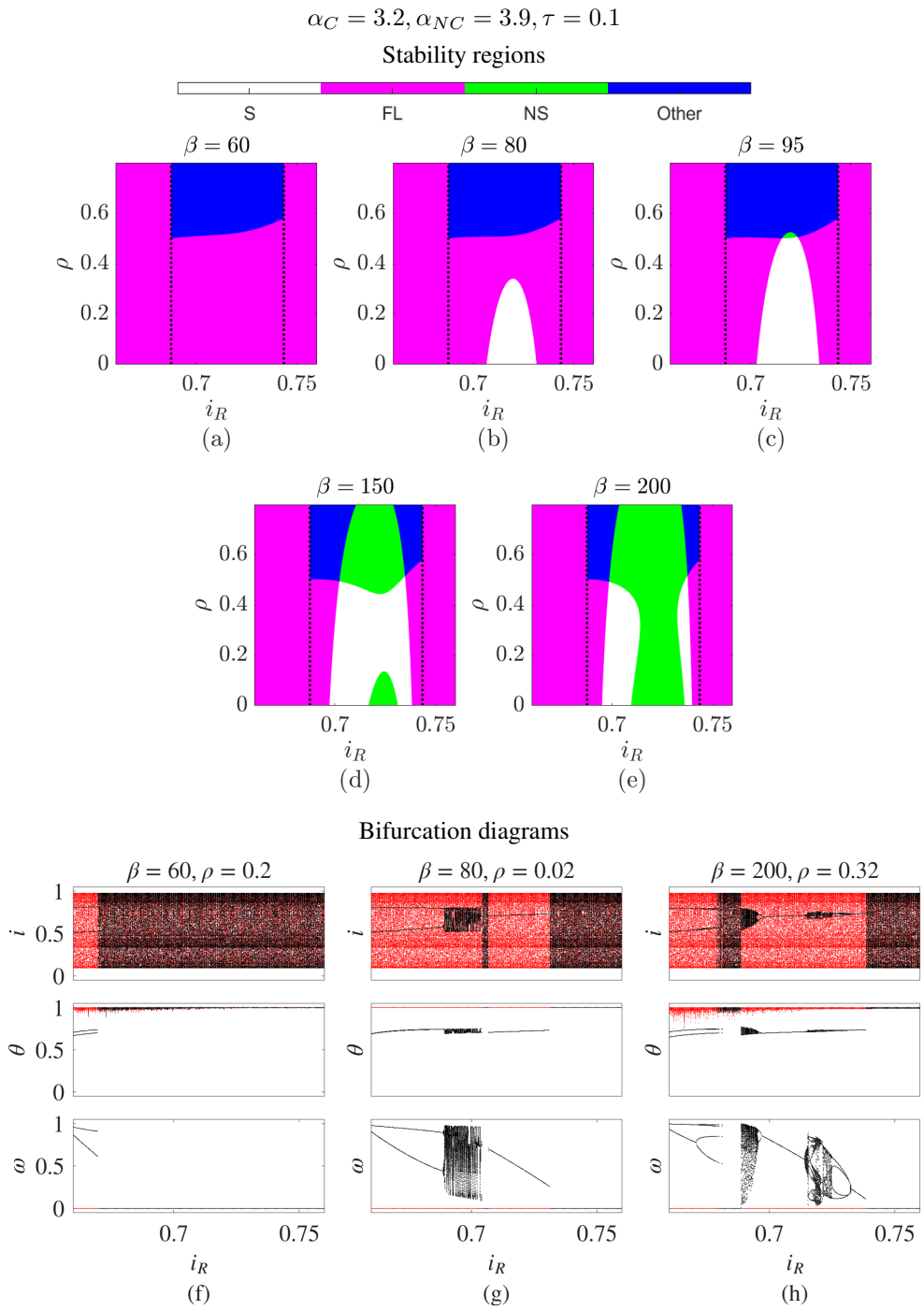

Figure 14: Case of unstable endemic steady states for both homogeneous population of cooperators and non-cooperators ($\alpha_C = 3.2$ and $\alpha_{NC} = 3.9$), with low reactivity $\tau = 0.1$. Panels (a)–(e): stability regions for different values of β. Panels (f)–(h): bifurcation diagrams on increasing i_R for different initial data (red and black).

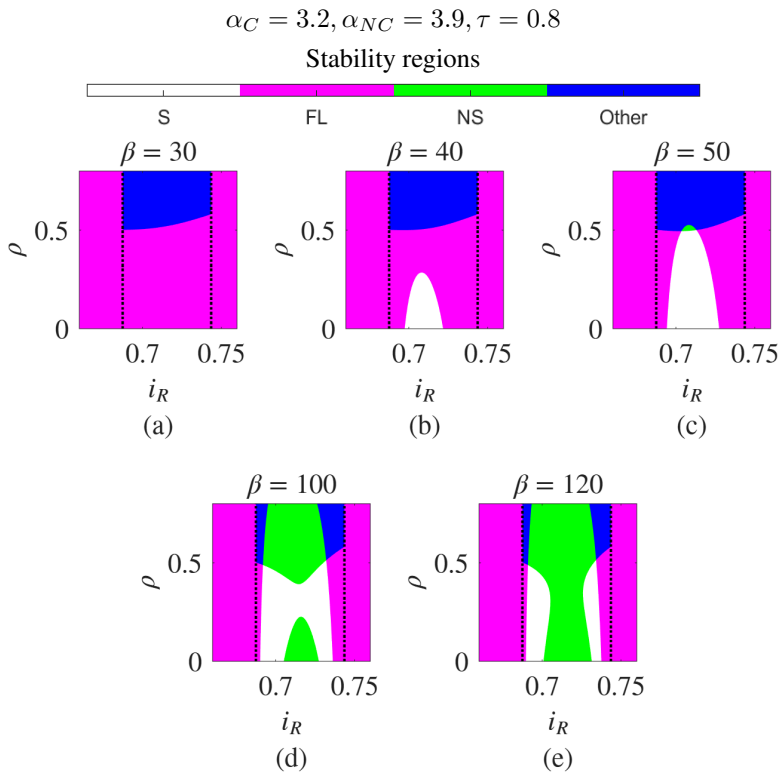

Figure 15: Case of unstable endemic steady states for both homogeneous population of cooperators and non-cooperators ($\alpha_C = 3.2$ and $\alpha_{NC} = 3.9$), with large reactivity $\tau = 0.8$. Panels (a)–(e): stability regions for different values of β.

of complexity, as highlighted by the red (in which the initial data are $i_0 = 0.8\, i_R$, $\theta_0 = 1 - 10^{-8}$ and $\omega_0 = 10^{-8}$) and black bifurcation diagrams in Panels (f)–(h) obtained on changing initial data.

The simulations for $\tau = 0.8$ are reported in Figure 15. Comparing the stability regions with those for $\tau = 0.1$ in Figures 14 (a)–(e) reveals that the overall behavior is essentially the same, with the only notable difference being a higher sensitivity to β when $\tau = 0.8$.

5 Conclusions

As we shall discuss below, the proposed model offers stimulating points for reflection, also in view of possible extensions. The interaction between the epidemiological and strategic spheres leads to a multiplicity of possible steady states, particularly endemic ones, showing that the scenario characterized by a share of infected individuals equal to i_R, as desired by the regulator, cannot always be achieved. What is interesting is that different (endemic) steady states are associated to different kinds of games, which both characterize and are based on the type of game that characterizes them. In the proposed setting, only symmetric games can emerge, and steady states are characterized by particular kinds of games: the coevolution between the epidemiological scenarios and the strategic interaction can explain, under an evolutionary setting, the emergence of cooperating and defecting attitudes.
Moreover, when steady states become unstable, in out-of-equilibrium dynamics the alternation of

different kinds of strategic interaction can emerge, giving rise to fluctuations between cooperating and non-cooperating behaviors.

The model we proposed can be extended in several directions. A first possibility might be given by the consideration of lock-in scenarios, i.e., allowing for the possibility that agents become trapped in situations in which the perceived alert threshold does not change, regardless of the circumstances. Such situations could arise depending on the formulation used to describe the evolution of the alert threshold, which might be altered with respect to that considered in the present work. See [23] for a general setting encompassing the one here proposed both in regard to the alert threshold evolution and the share updating rule. A second future line of research would consist in studying the effect of the introduction of uncertainty in the model, supposing that the perception of the alert threshold becomes a random variable in the presence of a multiplicity of signals (e.g., in regard to the actual efficacy of the implemented containment measures). For instance, we could assume that uncertainty affects the payoffs obtained by cooperating and defecting individuals, making them increase or fall, according to different effect combinations.
A further development of the proposed setting would be represented by an endogenization of the infection rates for cooperating and defecting individuals, which, rather than being constant, could represent strategies in an evolutive competition.
Analyzing the possible configurations of steady states, their stability, and their characterization in terms of strategic interactions in these three new settings will be the objective of the next steps in our research. A preliminary description and investigation of the settings with lock-in states and uncertainty can be found in [23].

Funding

The authors gratefully acknowledge the financial support of the European Union - Next Generation EU, Project PRIN 2022 "Evolutionary Poisson Games: Theory and Applications" (project code 2022BNPZY3, CUP H53D23002330006).

Appendix

Proof of Propositions 1 and 2. Setting $i_{t+1} = i_t = i$, $\theta_{t+1} = \theta_t = \theta$ and $\omega_{t+1} = \omega_t = \omega$, System (15) becomes

$$\begin{cases} i = i[1 - \gamma + (1-i)(\alpha_{NC} - (\alpha_{NC} - \alpha_C)\omega)] \\ F_2(\theta, \rho(i_R - i)) = 0 \\ \omega = \dfrac{\omega}{\omega + (1-\omega)e^{\beta(i-\theta)(\sigma - \omega(\tau+\sigma))}} \end{cases} \tag{27}$$

where in the second equation the expression of F_2 is that in (14). The first equation is solved for $i = 0$ and $i = 1 - \frac{\gamma}{\alpha_C\omega + \alpha_{NC}(1-\omega)}$.

Recalling (14) and (12), the second equation is solved for $i = i_R$ for any $\theta \in [0, 1]$, $\theta = 0$ for $i_R - i < 0$ and $\theta = 1$ for $i_R - i > 0$.

The third equation is solved for $\omega = 0,\ 1$ and for $\omega \in (0, 1)$ when

$$(i - \theta)[(\sigma + \tau)\omega - \sigma] = 0,$$

which provides $i = \theta$ and $\omega = \frac{\sigma}{\sigma+\tau}$, which, however, is not feasible as it never belongs to $(0, 1)$.

Hence, if $i = 0$, at a steady state the second equation in (27), since $i_R > 0$, requires $\theta = 1$, and hence the third equation is solved only for $\omega = 0$ or $\omega = 1$. We then have disease-free steady states $(0, 1, 0)$ and $(0, 1, 1)$.

Let us now consider endemic steady states, namely $i = 1 - \frac{\gamma}{\alpha_C\omega+\alpha_{NC}(1-\omega)} \in (0,1)$. In this case, we have to distinguish between the scenarios with $\omega = 0$, $\omega = 1$ and $i = \theta$.
If $\omega = 0$, then $i = 1 - \frac{\gamma}{\alpha_{NC}} \in (0,1)$ for $\gamma < \alpha_{NC}$ and the second equation in (27) requires

$$F_2\left(\theta, \rho\left(i_R - \left(1 - \frac{\gamma}{\alpha_{NC}}\right)\right)\right) = 0.$$

Recalling (11), if $i_R = 1 - \frac{\gamma}{\alpha_{NC}}$, then $z = i_R - \left(1 - \frac{\gamma}{\alpha_{NC}}\right) = 0 \in [-f_0^{-1}(\theta), f_0^{-1}(\theta)]$ for any θ. Hence, $F_2(\theta, 0) = f_0\big(f_0^{-1}(\theta)\big) - \theta = 0$, and therefore the second equation is satisfied for all $\theta \in [0,1]$. Conversely, if $i_R < 1 - \frac{\gamma}{\alpha_{NC}}$, that is, $i_R - \left(1 - \frac{\gamma}{\alpha_{NC}}\right) < 0 = f^{-1}(0)$, then, by (11), equation $F_2\left(\theta,\, i_R - \left(1 - \frac{\gamma}{\alpha_{NC}}\right)\right) = 0$ reduces to $1 - \theta = 0$, and it is solved for $\theta = 1$.

If $\omega = 1$, then $i = 1 - \frac{\gamma}{\alpha_C} \in (0,1)$ for $\gamma < \alpha_C$ and proceeding along the same lines as in the previous case, we find that if $i_R = 1 - \frac{\gamma}{\alpha_C}$ the second equation in (27) is fulfilled for any $\theta \in [0,1]$, while otherwise it is solved for $\theta = 0$ if $i_R < 1 - \frac{\gamma}{\alpha_C}$ and for $\theta = 1$ if $i_R > 1 - \frac{\gamma}{\alpha_C}$.

The second equation requires $F_2\left(\theta, \rho\left(i_R - \left(1 - \frac{\gamma}{\alpha_C}\right)\right)\right) = 0$, which is fulfilled for any $\theta \in [0,1]$ if $i_R = 1 - \frac{\gamma}{\alpha_C}$, while otherwise it is solved for $\theta = 0$ if $i_R < 1 - \frac{\gamma}{\alpha_C}$ and for $\theta = 1$ if $i_R > 1 - \frac{\gamma}{\alpha_C}$.

Finally, if $i = 1 - \frac{\gamma}{\alpha_C\omega+\alpha_{NC}(1-\omega)} = \theta \in (0,1)$, solutions $\theta = 0$ and $\theta = 1$ to $F_2(\theta, \rho(i_R - i)) = 0$ are excluded, and it can only be $i = i_R$, from which we find $\left(i_R, i_R, \frac{\alpha_{NC} - \frac{\gamma}{1-i_R}}{\alpha_{NC}-\alpha_C}\right)$ for $\alpha_C < \frac{\gamma}{1-i_R} < \alpha_{NC}$, where the expression for ω_R^* derives from the condition $i_R = 1 - \frac{\gamma}{\alpha_C\omega+\alpha_{NC}(1-\omega)}$.
This completes the proof. □

We only provide the proof of Proposition 4, as that of Proposition 3 follows by analogous steps.

Proof of Proposition 4. To obtain the payoff matrix in Table 1 at the steady states, i.e.

	C	NC
C	$1,1$	$\mathcal{S},\mathcal{T}$
NC	$\mathcal{T},\mathcal{S}$	$0,0$

it is sufficient to replace the various steady state components of i and θ in (9), so as to find the corresponding value of $\mathcal{T}$ and $\mathcal{S}$, together with their variation range, recalling that τ, $|\sigma| \in (0,1)$.
• $\boldsymbol{\xi}_R^*$: Using $i = i_R$ and $\theta = i_R$ in (9), we find $\mathcal{T} = 1$ and $\mathcal{S} = 0$.
• $\boldsymbol{\xi}_C^*$: Using $i = 1 - \frac{\gamma}{\alpha_C}$ and $\theta = 0$ in (9), we find $\mathcal{T} = 1 - \tau\left(1 - \frac{\gamma}{\alpha_C}\right)$ and $\mathcal{S} = -\sigma\left(1 - \frac{\gamma}{\alpha_C}\right)$. Recalling existence condition $\gamma < (1 - i_R)\alpha_C < \alpha_C$, we obtain ranges for $\mathcal{T}$ and $\mathcal{S}$.
• $\boldsymbol{\xi}_{NC}^*$: Using $i = 1 - \frac{\gamma}{\alpha_{NC}}$ and $\theta = 1$ in (9), we find $\mathcal{T} = 1 + \tau\frac{\gamma}{\alpha_{NC}}$ and $\mathcal{S} = \sigma\frac{\gamma}{\alpha_{NC}}$. Recalling existence condition $(1 - i_R)\alpha_{NC} < \gamma < \alpha_{NC}$, we obtain ranges for $\mathcal{T}$ and $\mathcal{S}$.
• $\left(1 - \frac{\gamma}{\alpha_C}, 1, 1\right)$: Using $i = 1 - \frac{\gamma}{\alpha_C}$ and $\theta = 1$ in (9), we find $\mathcal{T} = 1 + \tau\frac{\gamma}{\alpha_C}$ and $\mathcal{S} = \sigma\frac{\gamma}{\alpha_C}$. Recalling existence condition $(1 - i_R)\alpha_C < \gamma < \alpha_C$, we obtain ranges for $\mathcal{T}$ and $\mathcal{S}$.
• $\left(1 - \frac{\gamma}{\alpha_{NC}}, 0, 0\right)$: Using $i = 1 - \frac{\gamma}{\alpha_{NC}}$ and $\theta = 0$ in (9), we find $\mathcal{T} = 1 - \tau\left(1 - \frac{\gamma}{\alpha_{NC}}\right)$ and $\mathcal{S} = -\sigma\left(1 - \frac{\gamma}{\alpha_{NC}}\right)$. Recalling existence condition $\gamma < (1 - i_R)\alpha_{NC} < \alpha_{NC}$, we obtain ranges for $\mathcal{T}$ and $\mathcal{S}$.

• $\tilde{\boldsymbol{\xi}}_C^*$: Using $i = i_R = 1 - \frac{\gamma}{\alpha_C}$ and θ in (9), we find $\mathcal{T} = 1 - \tau\left(1 - \frac{\gamma}{\alpha_C} - \theta\right)$ and $\mathcal{S} = -\sigma\left(1 - \frac{\gamma}{\alpha_C} - \theta\right)$. Recalling existence condition $\gamma < \alpha_C$, we have

$$-1 < -\frac{\gamma}{\alpha_C} < 1 - \frac{\gamma}{\alpha_C} - \theta < 1 - \theta < 1,$$

from which we obtain the values that can be assumed by $\mathcal{T}$ and $\mathcal{S}$.
• $\tilde{\boldsymbol{\xi}}_{NC}^*$: Using $i = i_R = 1 - \frac{\gamma}{\alpha_{NC}}$ and θ in (9), we find $\mathcal{T} = 1 - \tau\left(1 - \frac{\gamma}{\alpha_{NC}} - \theta\right)$ and $\mathcal{S} = -\sigma\left(1 - \frac{\gamma}{\alpha_{NC}} - \theta\right)$. Proceeding as for $\tilde{\boldsymbol{\xi}}_C^*$, we obtain the values that can be assumed by $\mathcal{T}$ and $\mathcal{S}$. □

Proof of Proposition 5. We start recalling that, with M_1 and M_3 considered in the paper, i.e.,

$$M_1(i, \theta, \omega) = i(1 - \gamma + (1 - i)(\alpha_{NC} - \omega(\alpha_{NC} - \alpha_C)))$$

and

$$M_3(i, \theta, \omega) = \frac{\omega}{\omega + (1 - \omega)e^{\beta(i-\theta)(\sigma - \omega(\tau+\sigma))}}$$

so that $\frac{\partial M_3}{\partial \theta} = -\frac{\partial M_3}{\partial i}$, we have

$$\frac{\partial M_1}{\partial i} = 1 - \gamma + (1 - 2i)(\alpha_{NC} - \omega(\alpha_{NC} - \alpha_C)), \quad \frac{\partial M_1}{\partial \theta} = 0, \quad \frac{\partial M_1}{\partial \omega} = -i(1 - i)(\alpha_{NC} - \alpha_C),$$

$$\frac{\partial M_3}{\partial i} = \frac{-\beta\omega(1-\omega)e^{\beta(i-\theta)(\sigma-\omega(\tau+\sigma))}(\sigma-\omega(\tau+\sigma))}{(\omega+(1-\omega)e^{\beta(i-\theta)(\sigma-\omega(\tau+\sigma))})^2}, \qquad \frac{\partial M_3}{\partial \theta} = \frac{\beta\omega(1-\omega)e^{\beta(i-\theta)(\sigma-\omega(\tau+\sigma))}(\sigma-\omega(\tau+\sigma))}{(\omega+(1-\omega)e^{\beta(i-\theta)(\sigma-\omega(\tau+\sigma))})^2},$$

$$\frac{\partial M_3}{\partial \omega} = \frac{e^{\beta(i-\theta)(\sigma-\omega(\tau+\sigma))}(1+\omega(1-\omega)\beta(i-\theta)(\tau+\sigma))}{(\omega+(1-\omega)e^{\beta(i-\theta)(\sigma-\omega(\tau+\sigma))})^2}.$$

Hence, the Jacobian matrix is given by

$$J(i, \theta, \omega) = \begin{pmatrix} \frac{\partial M_1}{\partial i} & 0 & \frac{\partial M_1}{\partial \omega} \\ \frac{\partial M_2}{\partial i} & \frac{\partial M_2}{\partial \theta} & \frac{\partial M_2}{\partial \omega} \\ \frac{\partial M_3}{\partial i} & -\frac{\partial M_3}{\partial i} & \frac{\partial M_3}{\partial \omega} \end{pmatrix} = \begin{pmatrix} \frac{\partial M_1}{\partial i} & 0 & \frac{\partial M_1}{\partial \omega} \\ \frac{\partial M_2}{\partial i} & \frac{\partial M_2}{\partial \theta} & 0 \\ \frac{\partial M_3}{\partial i} & -\frac{\partial M_3}{\partial i} & \frac{\partial M_3}{\partial \omega} \end{pmatrix}$$

where, since $M_2(i, \theta, \omega) = \theta + F_2(\theta, \rho(i_R - i))$, we used $\frac{\partial M_2}{\partial \omega} = 0$.

Moreover, for (i, θ, ω) with $\omega = 0$ or $\omega = 1$ we have that $\frac{\partial M_3}{\partial \theta} = -\frac{\partial M_3}{\partial i} = 0$, so that in such cases the Jacobian matrix becomes

$$J(i, \theta, \omega) = \begin{pmatrix} \frac{\partial M_1}{\partial i} & 0 & \frac{\partial M_1}{\partial \omega} \\ \frac{\partial M_2}{\partial i} & \frac{\partial M_2}{\partial \theta} & 0 \\ 0 & 0 & \frac{\partial M_3}{\partial \omega} \end{pmatrix}. \tag{28}$$

Hence, a simple computation shows that the three eigenvalues of J coincide with $\frac{\partial M_1}{\partial i}$, $\frac{\partial M_2}{\partial \theta}$ and $\frac{\partial M_3}{\partial \omega}$. Let us then evaluate such partial derivatives at $\boldsymbol{\xi}_C^*$ and at $\boldsymbol{\xi}_{NC}^*$.
Computing them at $\boldsymbol{\xi}_C^*$, we find $\frac{\partial M_1}{\partial i} = 1 + \gamma - \alpha_C$, which lies in the interval $(-1, 1)$ for $\gamma > \alpha_C - 2$, and $\frac{\partial M_3}{\partial \omega} = e^{-\beta\tau\left(1 - \frac{\gamma}{\alpha_C}\right)}$, which always lies in the interval $(-1, 1)$. As concerns $\frac{\partial M_2}{\partial \theta}$, with F_2 in (14), since at $\boldsymbol{\xi}_C^*$ it must be $\gamma < (1 - i_R)\alpha_C$, and this implies that $z = \rho(i_R - i) <$

$0 = -1+\sqrt{1-\sqrt{\theta}}$ at $\boldsymbol{\xi}^*_C$, by continuity we have that $M_2(i,\theta,w) = \theta - \theta = 0$ in a neighborhood of $\boldsymbol{\xi}^*_C$, implying that $\frac{\partial M_2}{\partial \theta} = 0$. This concludes the proof for $\boldsymbol{\xi}^*_C$.
Turning now to $\boldsymbol{\xi}^*_{NC}$, we find $\frac{\partial M_1}{\partial i} = 1 + \gamma - \alpha_{NC}$, which lies in the interval $(-1,1)$ for $\gamma > \alpha_{NC} - 2$, and $\frac{\partial M_3}{\partial \omega} = e^{\beta\sigma\frac{\gamma}{\alpha_{NC}}}$, which always lies in the interval $(-1,1)$.
For $\frac{\partial M_2}{\partial \theta}$, with F_2 in (14), since at $\boldsymbol{\xi}^*_{NC}$ it must be $\gamma > (1-i_R)\alpha_{NC}$, and this implies that $z = \rho(i_R - i) > 0 = \sqrt{1-\sqrt{\theta}}$ at $\boldsymbol{\xi}^*_{NC}$, by continuity we have that $M_2(i,\theta,\omega) = \theta + 1 - \theta = 1$ in a neighborhood of $\boldsymbol{\xi}^*_{NC}$, implying that $\frac{\partial M_2}{\partial \theta} = 0$. This concludes the proof for $\boldsymbol{\xi}^*_{NC}$, too. □

Proof of Propositions 6 and 7. Recalling (28) and the subsequent lines, it holds that, at the steady states considered in Propositions 6 and 7, the three eigenvalues of J coincide with $\frac{\partial M_1}{\partial i}$, $\frac{\partial M_2}{\partial \theta}$ and $\frac{\partial M_3}{\partial \omega}$. Let us then evaluate such partial derivatives at the various steady states.
At $\left(1-\frac{\gamma}{\alpha_C}, 1, 1\right)$ it holds that $\frac{\partial M_3}{\partial \omega} = e^{\frac{\beta\tau\gamma}{\alpha_C}}$, which is always greater than 1, implying that this steady state is unstable.
Similarly, at $\left(1-\frac{\gamma}{\alpha_{NC}}, 0, 0\right)$ it holds that $\frac{\partial M_3}{\partial \omega} = e^{-\beta\sigma\left(1-\frac{\gamma}{\alpha_{NC}}\right)}$, which, since $\sigma < 0$, is always greater than 1, implying the instability for the corresponding steady state.
In an analogous manner, at $(0,1,1)$ it holds that $\frac{\partial M_3}{\partial \omega} = e^{\beta\tau} > 1$ so that the steady state is unstable.
On the other hand, at $\boldsymbol{\xi}^*_{df} = (0,1,0)$ it holds that $\frac{\partial M_3}{\partial \omega} = e^{\beta\sigma}$ always lies in the interval $(0,1)$, while $\frac{\partial M_1}{\partial i} = 1 - \gamma + \alpha_{NC} \in (-1,1)$ if and only if $\alpha_{NC} < \gamma$. As concerns $\frac{\partial M_2}{\partial \theta}$ at $\boldsymbol{\xi}^*_{df}$, with F_2 in (14), since $z = \rho(i_R - i) = \rho i_R > 0 = \sqrt{1-\sqrt{\theta}}$ at $\boldsymbol{\xi}^*_{df}$, by continuity we have that $M_2(i,\theta,\omega) = \theta + 1 - \theta = 1$ in a neighborhood of $\boldsymbol{\xi}^*_{df}$, implying that $\frac{\partial M_2}{\partial \theta} = 0$. Hence, $\boldsymbol{\xi}^*_{df}$ is locally asymptotically stable for $\gamma > \alpha_{NC}$, as desired. □

Proof of Proposition 8. Recalling (28) and the subsequent lines, it holds that $\frac{\partial M_1}{\partial i}$ and $\frac{\partial M_3}{\partial \omega}$ are eigenvalues of the Jacobian matrix of the model along the two considered continua of steady states.
Let us focus on $\tilde{\boldsymbol{\xi}}^*_C$, noting that $\frac{\partial M_1}{\partial i}\left(1-\frac{\gamma}{\alpha_C}, \theta, 1\right) = 1 + \gamma - \alpha_C$ is less than -1 if $\gamma < \alpha_C - 2$.
Moreover, $\frac{\partial M_3}{\partial \omega}\left(1-\frac{\gamma}{\alpha_C}, \theta, 1\right) = e^{\beta\tau\left(\theta - 1 + \frac{\gamma}{\alpha_C}\right)}$ is strictly greater than 1 if $\theta > 1 - \frac{\gamma}{\alpha_C}$.
Let us now focus on $\tilde{\boldsymbol{\xi}}^*_{NC}$, observing that $\frac{\partial M_1}{\partial i}\left(1-\frac{\gamma}{\alpha_{NC}}, \theta, 0\right) = 1 + \gamma - \alpha_{NC}$ is less than -1 if $\gamma < \alpha_{NC} - 2$. Moreover, $\frac{\partial M_3}{\partial \omega}\left(1-\frac{\gamma}{\alpha_{NC}}, \theta, 0\right) = e^{-\beta\sigma\left(1-\frac{\gamma}{\alpha_{NC}} - \theta\right)}$ is larger than 1 if $\theta < 1 - \frac{\gamma}{\alpha_{NC}}$. □

In view of the computations in the proof of Lemma 1, we note that the smoothness of (14) guarantees that

$$\frac{\partial F_2(\theta,z)}{\partial z} = \begin{cases} 0 & z < -f_0^{-1}(\theta) \\ 4(z + f_0^{-1}(\theta))(1 - z - f_0^{-1}(\theta))(2 - z - f_0^{-1}(\theta)) & z \in [-f_0^{-1}(\theta), 1 - f_0^{-1}(\theta)] \\ 0 & z > 1 - f_0^{-1}(\theta) \end{cases}$$

where $f_0^{-1}(\theta)$ is given by (13) , smoothly approaches 0 as $\rho(i_R - i_t)$ approaches the values $-1 + \sqrt{1-\sqrt{\theta}}$ and $\sqrt{1-\sqrt{\theta}}$. Moreover, it holds that

$$\frac{\partial F_2(i_R,0)}{\partial z} = 4\sqrt{i_R\left(1-\sqrt{i_R}\right)}\,. \tag{29}$$

Lemma 1. *Steady state* $\boldsymbol{\xi}_R^* = \left(i_R, i_R, \frac{\alpha_{NC} - \frac{\gamma}{1-i_R}}{\alpha_{NC} - \alpha_C}\right)$, *when it exists for* $\alpha_C < \frac{\gamma}{1-i_R} < \alpha_{NC}$, *is locally asymptotically stable if*

$$\frac{\gamma i_R}{1-i_R} - 4\rho\sqrt{i_R\left(1-\sqrt{i_R}\right)}\left(1+\frac{\gamma i_R}{1-i_R}\right) - \frac{\beta\, i_R(1-i_R)}{(\alpha_{NC}-\alpha_C)^2}\left(4\rho\sqrt{i_R\left(1-\sqrt{i_R}\right)}-1\right)^2 A > 0, \quad (30)$$

$$2\left(2-\frac{\gamma i_R}{1-i_R}\right) - \frac{\beta\, i_R(1-i_R)}{(\alpha_{NC}-\alpha_C)^2}\left(2\rho\sqrt{i_R\left(1-\sqrt{i_R}\right)}-1\right)A > 0$$

and

$$\frac{2\gamma}{1-i_R} - \frac{\beta\,(1-i_R)A}{(\alpha_{NC}-\alpha_C)^2} > 0. \quad (31)$$

Proof of Lemma 1. Recalling the expression for the partial derivatives for M_1 and M_3 reported in the proof of Proposition 5, at $\boldsymbol{\xi}_R^*$ we have

$$\frac{\partial M_1}{\partial i} = 1 - \frac{\gamma i_R}{1-i_R}, \qquad \frac{\partial M_1}{\partial \theta} = 0, \qquad \frac{\partial M_1}{\partial \omega} = -i_R(1-i_R)(\alpha_{NC}-\alpha_C),$$

$$\frac{\partial M_3}{\partial i} = \frac{\beta A}{(\alpha_{NC}-\alpha_C)^3}, \qquad \frac{\partial M_3}{\partial \theta} = -\frac{\beta A}{(\alpha_{NC}-\alpha_C)^3}, \qquad \frac{\partial M_3}{\partial \omega} = 1.$$

Moreover, with F_2 in (14), recalling also (29), at $\boldsymbol{\xi}_R^*$ we have

$$\frac{\partial M_2}{\partial i} = -4\rho\sqrt{i_R\left(1-\sqrt{i_R}\right)}, \quad \frac{\partial M_2}{\partial \theta} = 1, \quad \frac{\partial M_2}{\partial \omega} = 0.$$

Hence, as coefficients of the characteristic polynomial $\lambda^3 + \chi_1\lambda^2 + \chi_2\lambda + \chi_3 = 0$ of the Jacobian matrix J of $\boldsymbol{M} = (M_1, M_2, M_3)$ computed at $\boldsymbol{\xi}_R^*$, we find

$\chi_1 = -\frac{\partial M_1}{\partial i} - \frac{\partial M_2}{\partial \theta} - \frac{\partial M_3}{\partial \omega} = -3 + \frac{\gamma i_R}{1-i_R}$,

$\chi_2 = \frac{\partial M_1}{\partial i}\frac{\partial M_2}{\partial \theta} + \frac{\partial M_2}{\partial \theta}\frac{\partial M_3}{\partial \omega} + \frac{\partial M_1}{\partial i}\frac{\partial M_3}{\partial \omega} - \frac{\partial M_1}{\partial \omega}\frac{\partial M_3}{\partial i} = 3 - 2\frac{\gamma i_R}{1-i_R} + \frac{\beta i_R(1-i_R)A}{(\alpha_{NC}-\alpha_C)^2}$,

$\chi_3 = -\frac{\partial M_1}{\partial i}\frac{\partial M_2}{\partial \theta}\frac{\partial M_3}{\partial \omega} + \frac{\partial M_1}{\partial \omega}\frac{\partial M_3}{\partial i}\left(\frac{\partial M_2}{\partial i} + \frac{\partial M_2}{\partial \theta}\right) = 1 + \frac{\gamma i_R}{1-i_R} + \frac{\beta i_R(1-i_R)A}{(\alpha_{NC}-\alpha_C)^2}\left(4\rho\sqrt{i_R\left(1-\sqrt{i_R}\right)}-1\right)$.

Let us now derive the Farebrother conditions

$$(i)\ 1-\chi_1+\chi_2-\chi_3 > 0; \qquad (ii)\ 1-\chi_2+\chi_1\chi_3-(\chi_3)^2 > 0;$$
$$(iii)\ 3-\chi_2 > 0; \qquad (iv)\ 1+\chi_1+\chi_2+\chi_3 > 0,$$

which together ensure that $\boldsymbol{\xi}_R^*$ is locally asymptotically stable.

It holds that (iv) can be rephrased as

$$4\rho A\sqrt{i_R\left(1-\sqrt{i_R}\right)} > 0, \quad (32)$$

that is always fulfilled, since $\alpha_C < \frac{\gamma}{1-i_R} < \alpha_{NC}$ at $\boldsymbol{\xi}_R^*$ and $\sigma < 0 < \tau$.

We now move to (i), which reads as

$$2\left(2 - \frac{\gamma i_R}{1-i_R}\right) - \frac{\beta\, i_R(1-i_R)}{(\alpha_{NC}-\alpha_C)^2}\left(2\rho\sqrt{i_R\left(1-\sqrt{i_R}\right)} - 1\right) A > 0,$$

while (iii) can be rewritten as

$$\frac{2\gamma}{1-i_R} - \frac{\beta\,(1-i_R)A}{(\alpha_{NC}-\alpha_C)^2} > 0. \tag{33}$$

Finally, we have that (ii) reads as

$$\frac{\gamma i_R}{1-i_R} - 4\rho\sqrt{i_R\left(1-\sqrt{i_R}\right)}\left(1 + \frac{\gamma i_R}{1-i_R}\right) - \frac{\beta\, i_R(1-i_R)}{(\alpha_{NC}-\alpha_C)^2}\left(4\rho\sqrt{i_R\left(1-\sqrt{i_R}\right)} - 1\right)^2 A > 0.$$

□

Proof of Proposition 9. Recalling the definition of $\tilde{\beta}$ in (17), we can rewrite the conditions in Lemma 1 as

$$\frac{\gamma i_R}{1-i_R} - 4\rho\sqrt{i_R\left(1-\sqrt{i_R}\right)}\left(1 + \frac{\gamma i_R}{1-i_R}\right) - \tilde{\beta}\left(4\rho\sqrt{i_R\left(1-\sqrt{i_R}\right)} - 1\right)^2 > 0, \tag{34}$$

$$2\left(2 - \frac{\gamma i_R}{1-i_R}\right) - \tilde{\beta}\left(2\rho\sqrt{i_R\left(1-\sqrt{i_R}\right)} - 1\right) > 0, \tag{35}$$

$$\frac{2\gamma i_R}{1-i_R} - \tilde{\beta} > 0. \tag{36}$$

Moreover, recalling the definition of $\tilde{\imath}_R$ in (26), after some algebraic manipulations, (34) can be written as

$$\phi\left(\rho\tilde{\imath}_R\right) := \tilde{\beta}(\rho\tilde{\imath}_R)^2 - \left[2\tilde{\beta} - 1 - \frac{\gamma i_R}{1-i_R}\right]\rho\tilde{\imath}_R + \tilde{\beta} - \frac{\gamma i_R}{1-i_R} < 0.$$

Let $\tilde{\rho}_{ns,1} < \tilde{\rho}_{ns,2}$ be the two possible solutions to $\phi\left(\rho\tilde{\imath}_R\right) = 0$ defined in (19). Since ϕ represents a convex parabola with $\phi(1) = 1 > 0$ and $\phi'(1) = 1 + \frac{\gamma i_R}{1-i_R} > 0$, it follows that $\tilde{\rho}_{ns,1}$ and $\tilde{\rho}_{ns,2}$, if they exist, are smaller than 1. The existence and position of $\tilde{\rho}_{ns,1}$ and $\tilde{\rho}_{ns,2}$ are determined by $\phi(0)$, $\phi'(0)$ and by the discriminant of ϕ. In particular, it holds that $\phi(0) = \tilde{\beta} - \frac{\gamma i_R}{1-i_R}$, so if $\phi(0) < 0$, namely if

$$\tilde{\beta} < \frac{\gamma i_R}{1-i_R}, \tag{37}$$

we have that $\phi\left(\rho\tilde{\imath}_R\right) < 0$ for $\rho\tilde{\imath}_R \in (0, \tilde{\rho}_{ns,2})$.

If $\phi(0) = 0$, i.e. if $\tilde{\beta} = \frac{\gamma i_R}{1-i_R}$, we have $\phi\left(\rho\tilde{\imath}_R\right) < 0$ for $\rho\tilde{\imath}_R \in (0, \tilde{\rho}_{ns,2})$ if $\phi'(0) < 0$, namely if $1 + \frac{\gamma i_R}{1-i_R} - 2\tilde{\beta} < 0$, or equivalently if $1 + \frac{\gamma i_R}{1-i_R} - 2\frac{\gamma i_R}{1-i_R} < 0$, which provides $\gamma > \frac{1-i_R}{i_R}$.

We have that $\phi\left(\rho\tilde{\imath}_R\right) = 0$ has no positive solutions if its discriminant is negative or null, namely if

$$\left(1 + \frac{\gamma i_R}{1-i_R}\right)^2 - 4\tilde{\beta} \leq 0,$$

i.e. if

$$\tilde{\beta} \geq \frac{1}{4}\left(1+\frac{\gamma i_R}{1-i_R}\right)^2, \tag{38}$$

in which case $\phi\left(\rho\tilde{\iota}_R\right) \geq 0$ for any $\rho\tilde{\iota}_R$.

Conversely, if $\phi(0) > 0$ and the discriminant is positive, which, recalling (37) and (38), amounts to

$$\frac{\gamma i_R}{1-i_R} < \tilde{\beta} < \frac{1}{4}\left(1+\frac{\gamma i_R}{1-i_R}\right)^2, \tag{39}$$

then it holds that $\phi\left(\rho\tilde{\iota}_R\right) < 0$ for $\rho\tilde{\iota}_R \in (\tilde{\rho}_{ns,1}, \tilde{\rho}_{ns,2})$. To have $\tilde{\rho}_{ns,1} > 0$, we must impose $\phi'(0) < 0$, which, combined with the rightmost inequality in (39), also in this case, requires $\gamma > \frac{1-i_R}{i_R}$. Note that this restriction implies that $\frac{\gamma i_R}{1-i_R} < \tilde{\beta} < \frac{1}{4}\left(1+\frac{\gamma i_R}{1-i_R}\right)^2$ is fulfilled.

Turning to (35), which can be rewritten as

$$2\left(2-\frac{\gamma i_R}{1-i_R}\right) - \tilde{\beta}\left(\frac{\rho\tilde{\iota}_R}{2}-1\right) > 0,$$

since for (34) we need $\rho\tilde{\iota}_R < \tilde{\rho}_{ns,2}$ and that $\tilde{\rho}_{ns,2} < 1$, we have $\frac{\rho\tilde{\iota}_R}{2} - 1 < 0$. This means that if $\gamma \leq \frac{2(1-i_R)}{i_R}$, then (35) is fulfilled. Conversely, if $\gamma > \frac{2(1-i_R)}{i_R}$, we need

$$\rho\tilde{\iota}_R < 2\left(1-\frac{2}{\tilde{\beta}}\left(\frac{\gamma i_R}{1-i_R}-2\right)\right) = \tilde{\rho}_{fl},$$

recalling (20).

Finally, (36) can be written as

$$\tilde{\beta} < \frac{2\gamma i_R}{1-i_R}.$$

Combining the various possibilities for the validity of (34), (35) and (36), we find that steady state $\boldsymbol{\xi}_R^*$ is locally asymptotically stable for

1. $\rho \in \left(0, \dfrac{\tilde{\rho}_{ns,2}}{4\sqrt{i_R\left(1-\sqrt{i_R}\right)}}\right)$ if

$$\begin{cases} \tilde{\beta} < \frac{\gamma i_R}{1-i_R} \\ \gamma \leq \frac{2(1-i_R)}{i_R} \end{cases} \tag{40}$$

or if

$$\begin{cases} \tilde{\beta} = \frac{i_R}{1-i_R} \\ \frac{i_R}{1-i_R} < \gamma \leq \frac{2(1-i_R)}{i_R} \end{cases} \tag{41}$$

2. $\rho \in \left(\dfrac{\tilde{\rho}_{ns,1}}{4\sqrt{i_R\left(1-\sqrt{i_R}\right)}}, \dfrac{\tilde{\rho}_{ns,2}}{4\sqrt{i_R\left(1-\sqrt{i_R}\right)}}\right)$ if

$$\begin{cases} \frac{\gamma i_R}{1-i_R} < \tilde{\beta} < \min\left\{\frac{1}{4}\left(1+\frac{\gamma i_R}{1-i_R}\right)^2, \frac{2\gamma i_R}{1-i_R}\right\} \\ \frac{1-i_R}{i_R} < \gamma \leq \frac{2(1-i_R)}{i_R} \end{cases} \tag{42}$$

3. $\rho \in \left(0, \dfrac{\min\{\tilde{\rho}_{ns,2}, \tilde{\rho}_{fl}\}}{4\sqrt{i_R\left(1-\sqrt{i_R}\right)}}\right)$ if

$$\begin{cases} \tilde{\beta} \leq \frac{\gamma i_R}{1-i_R} \\ \gamma > \frac{2(1-i_R)}{i_R} \end{cases} \tag{43}$$

4. $\rho \in \left(\dfrac{\tilde{\rho}_{ns,1}}{4\sqrt{i_R\left(1-\sqrt{i_R}\right)}}, \dfrac{\min\{\tilde{\rho}_{ns,2}, \tilde{\rho}_{fl}\}}{4\sqrt{i_R\left(1-\sqrt{i_R}\right)}}\right)$ if

$$\begin{cases} \frac{\gamma i_R}{1-i_R} < \tilde{\beta} < \min\left\{\frac{1}{4}\left(1+\frac{\gamma i_R}{1-i_R}\right)^2, \frac{2\gamma i_R}{1-i_R}\right\} \\ \gamma > \frac{2(1-i_R)}{i_R} \end{cases} \tag{44}$$

In order to check the compatibility of the above set of conditions, recalling that $\gamma \leq 1$ and $i_R \in (0,1)$, we start noting that

$$\frac{2(1-i_R)}{i_R} \geq 1 \;\Leftrightarrow\; i_R \leq \frac{2}{3}. \tag{45}$$

We focus on Case 1 above.
From the first condition in System (40) we have $\beta < \beta_0$, while the second condition, recalling (45), is unnecessary for $i_R \in \left(0, \frac{2}{3}\right]$, otherwise we keep it.
From the first condition in System (41) we have $\beta = \beta_0$, whereas condition $\gamma \leq \frac{2(1-i_R)}{i_R}$, recalling (45), is fulfilled for $i_R \in \left(0, \frac{2}{3}\right]$.
In such manner, we obtain the statement in Case 1 of the present proposition.

Now we focus on Case 2 above.
From the first condition in System (42) we obtain $\beta_0 < \beta < \min\{2\beta_0, \beta_\delta\}$.
Hence, recalling (45), we can split System (42) into

$$\begin{cases} i_R \in \left(0, \frac{2}{3}\right] \\ 4\rho\sqrt{i_R\left(1-\sqrt{i_R}\right)} \in (\tilde{\rho}_{ns,1}, \tilde{\rho}_{ns,2}) \\ \beta_0 < \beta < \min\{2\beta_0, \beta_\delta\} \\ \gamma > \frac{1-i_R}{i_R} \end{cases} \vee \begin{cases} i_R \in \left(\frac{2}{3}, 1\right) \\ 4\rho\sqrt{i_R\left(1-\sqrt{i_R}\right)} \in (\tilde{\rho}_{ns,1}, \tilde{\rho}_{ns,2}) \\ \beta_0 < \beta < \min\{2\beta_0, \beta_\delta\} \\ \gamma \leq \frac{2(1-i_R)}{i_R} \\ \gamma > \frac{1-i_R}{i_R} \end{cases} \tag{46}$$

Recalling that by [24] it is not possible that (iii) in Farebrother conditions (cf. the proof of Lemma 1) holds with an equality while the remaining conditions are fulfilled, we shall add, in all systems in (46), the condition $\beta_\delta \leq 2\beta_0$, which is equivalent to $\frac{\left(1+\frac{\gamma i_R}{1-i_R}\right)^2}{4i_R} \leq \frac{2\gamma}{1-i_R}$, i.e., to $\gamma \in [\gamma_a, \gamma_b]$, with $\gamma_{a,b} = \frac{(3\pm\sqrt{8})(1-i_R)}{i_R}$.
Since it holds that $\gamma_a < \frac{1-i_R}{i_R}$, then γ_a will not play any role. As concerns instead γ_b, it holds that $\gamma_b < 1$ for $i_R > \frac{3+\sqrt{8}}{4+\sqrt{8}} > \frac{2}{3}$. Moreover, since $\frac{1-i_R}{i_R} < 1$ for $i_R > \frac{1}{2}$, the first system in (46) can be rewritten as

$$\begin{cases} i_R \in \left(\frac{1}{2}, \frac{2}{3}\right] \\ 4\rho\sqrt{i_R\left(1-\sqrt{i_R}\right)} \in (\tilde{\rho}_{ns,1}, \tilde{\rho}_{ns,2}) \\ \beta_0 < \beta < \beta_\delta \\ \gamma \in \left(\frac{1-i_R}{i_R}, 1\right] \end{cases}$$

and provides the first statement in Case 2 of the present proposition.
The second system in (46) can instead be rewritten as

$$\begin{cases} i_R \in \left(\frac{2}{3}, 1\right) \\ 4\rho\sqrt{i_R\left(1-\sqrt{i_R}\right)} \in (\tilde{\rho}_{ns,1}, \tilde{\rho}_{ns,2}) \\ \beta_0 < \beta < \beta_\delta \\ \gamma \in \left(\frac{1-i_R}{i_R}, \frac{2(1-i_R)}{i_R}\right] \\ \gamma \in [\gamma_a, \gamma_b] \end{cases}$$

Since $\gamma_a < \frac{1-i_R}{i_R} < \frac{2(1-i_R)}{i_R} < \gamma_b$, the system is equivalent to

$$\begin{cases} i_R \in \left(\frac{2}{3}, 1\right) \\ 4\rho\sqrt{i_R\left(1-\sqrt{i_R}\right)} \in (\tilde{\rho}_{ns,1}, \tilde{\rho}_{ns,2}) \\ \beta_0 < \beta < \beta_\delta \\ \gamma \in \left(\frac{1-i_R}{i_R}, \frac{2(1-i_R)}{i_R}\right] \end{cases}$$

which provides the second statement in Case 2 of the present proposition.

Now we focus on Case 3 above.
From the first condition in System (43) we find $\beta \leq \beta_0$. Recalling that from (45) the second condition is possible only if $i_R > \frac{2}{3}$, we obtain statement in Case 3 of the present proposition.

Finally, we focus on Case 4 above.
From the first condition in System (44) we find $\beta_0 < \beta < \min\{2\beta_0, \beta_\delta\}$.
Recalling the discussion about the solution to Case 2 above, the resulting system can be split as

$$\begin{cases} i_R \in \left(\frac{2}{3}, \frac{3+\sqrt{8}}{4+\sqrt{8}}\right] \\ 4\rho\sqrt{i_R\left(1-\sqrt{i_R}\right)} \in (\tilde{\rho}_{ns,1}, \tilde{\rho}_{ns,2}) \\ 4\rho\sqrt{i_R\left(1-\sqrt{i_R}\right)} < \tilde{\rho}_{fl} \\ \beta_0 < \beta < \beta_\delta \\ \gamma > \frac{2(1-i_R)}{i_R} \\ \gamma \in \left[\frac{(3-\sqrt{8})(1-i_R)}{i_R}, 1\right] \end{cases} \quad \vee \quad \begin{cases} i_R \in \left(\frac{3+\sqrt{8}}{4+\sqrt{8}}, 1\right) \\ 4\rho\sqrt{i_R\left(1-\sqrt{i_R}\right)} \in (\tilde{\rho}_{ns,1}, \tilde{\rho}_{ns,2}) \\ 4\rho\sqrt{i_R\left(1-\sqrt{i_R}\right)} < \tilde{\rho}_{fl} \\ \beta_0 < \beta < \beta_\delta \\ \gamma > \frac{2(1-i_R)}{i_R} \\ \gamma \in \left[\frac{(3-\sqrt{8})(1-i_R)}{i_R}, \frac{(3+\sqrt{8})(1-i_R)}{i_R}\right] \end{cases}$$

or, equivalently, as

$$\begin{cases} i_R \in \left(\frac{2}{3}, \frac{3+\sqrt{8}}{4+\sqrt{8}}\right] \\ 4\rho\sqrt{i_R\left(1-\sqrt{i_R}\right)} \in (\tilde{\rho}_{ns,1}, \tilde{\rho}_{ns,2}) \\ 4\rho\sqrt{i_R\left(1-\sqrt{i_R}\right)} < \tilde{\rho}_{fl} \\ \beta_0 < \beta < \beta_\delta \\ \gamma > \frac{2(1-i_R)}{i_R} \end{cases} \quad \vee \quad \begin{cases} i_R \in \left(\frac{3+\sqrt{8}}{4+\sqrt{8}}, 1\right) \\ 4\rho\sqrt{i_R\left(1-\sqrt{i_R}\right)} \in (\tilde{\rho}_{ns,1}, \tilde{\rho}_{ns,2}) \\ 4\rho\sqrt{i_R\left(1-\sqrt{i_R}\right)} < \tilde{\rho}_{fl} \\ \beta_0 < \beta < \beta_\delta \\ \gamma \in \left(\frac{2(1-i_R)}{i_R}, \frac{(3+\sqrt{8})(1-i_R)}{i_R}\right] \end{cases}$$

which is statement in Case 4 of the present proposition and concludes the proof. □

Proof of Proposition 10. We rewrite the first two conditions in Lemma 1 as

$$\frac{\gamma i_R}{1-i_R} - \rho\tilde{\iota}_R\left(1+\frac{\gamma i_R}{1-i_R}\right) - \frac{\beta\, i_R(1-i_R)}{(\alpha_{NC}-\alpha_C)^2}\left(1-\rho\tilde{\iota}_R\right)^2 A > 0 \tag{47}$$

and

$$2\left(2-\frac{\gamma i_R}{1-i_R}\right) + \frac{\beta\, i_R(1-i_R)}{(\alpha_{NC}-\alpha_C)^2}\left(1-\frac{\rho\tilde{\iota}_R}{2}\right) A > 0, \tag{48}$$

with $\rho\tilde{\iota}_R$ as in (26), while we keep (31) unchanged.

Recalling the definition of β_0 in (21), we start noting that (31) is satisfied for $\beta < 2\beta_0$.

Turning to (47), it is fulfilled for $\beta < \beta_{ns}$, with β_{ns} in (25), and this requires $\rho\tilde{\iota}_R < \hat{\rho}$, with $\hat{\rho}$ introduced in (22), i.e., recalling (26), for $\rho < \frac{\hat{\rho}}{4\sqrt{i_R\left(1-\sqrt{i_R}\right)}}$. According to the proof of Proposition 9, any $\rho\tilde{\iota}_R$ satisfying (30), and thus (47), must lie in $(0,1)$, and this is the case by imposing $\rho\tilde{\iota}_R < \hat{\rho}$, since $\hat{\rho} < 1$.

Finally, (48) is satisfied for $\beta > \beta_{fl}$, with β_{fl} in (24), when the latter is positive, i.e., for $\gamma > \frac{2(1-i_R)}{i_R}$, while (48) is always fulfilled if $\gamma \leq \frac{2(1-i_R)}{i_R}$.

Hence, (31), (47) and (48) are satisfied in the following cases:

$$\begin{cases} \gamma \leq \frac{2(1-i_R)}{i_R} \\ \rho\tilde{\iota}_R < \hat{\rho} \\ \beta < \beta_{ns} \\ \beta < 2\beta_0 \end{cases} \quad \vee \quad \begin{cases} \gamma > \frac{2(1-i_R)}{i_R} \\ \rho\tilde{\iota}_R < \hat{\rho} \\ \beta > \beta_{fl} \\ \beta < \beta_{ns} \\ \beta < 2\beta_0 \end{cases} \tag{49}$$

Recalling that (see e.g. [24]) it is not possible that (iii) in Farebrother conditions (cf. the proof of Lemma 1), i.e., (31), holds with an equality while the remaining conditions are satisfied, we have to add the condition $\beta_{ns} \leq 2\beta_0$ in both systems in (49), thus obtaining

$$\begin{cases} \gamma \leq \frac{2(1-i_R)}{i_R} \\ \rho\tilde{\iota}_R < \hat{\rho} \\ \beta < \beta_{ns} \\ \beta_{ns} \leq 2\beta_0 \end{cases} \quad \vee \quad \begin{cases} \gamma > \frac{2(1-i_R)}{i_R} \\ \rho\tilde{\iota}_R < \hat{\rho} \\ \beta > \beta_{fl} \\ \beta < \beta_{ns} \\ \beta_{ns} \leq 2\beta_0 \end{cases} \tag{50}$$

Noting that $\frac{2(1-i_R)}{i_R} \geq 1$ for $i_R \leq \frac{2}{3}$, and recalling that $\gamma \leq 1$ and $i_R \in (0,1)$, then the systems in (50) can be rewritten as

$$\begin{cases} i_R \in (0, \frac{2}{3}] \\ \rho\tilde{\iota}_R < \hat{\rho} \\ \beta < \beta_{ns} \\ \beta_{ns} \leq 2\beta_0 \end{cases} \quad \vee \quad \begin{cases} i_R \in (\frac{2}{3}, 1) \\ \gamma \leq \frac{2(1-i_R)}{i_R} \\ \rho\tilde{\iota}_R < \hat{\rho} \\ \beta < \beta_{ns} \\ \beta_{ns} \leq 2\beta_0 \end{cases} \quad \vee \quad \begin{cases} i_R \in (\frac{2}{3}, 1) \\ \frac{2(1-i_R)}{i_R} < \gamma \leq 1 \\ \rho\tilde{\iota}_R < \hat{\rho} \\ \beta > \beta_{fl} \\ \beta < \beta_{ns} \\ \beta_{ns} \leq 2\beta_0 \end{cases} \tag{51}$$

Comparing the thresholds found for β in (21) and (25), we find that $\beta_{ns} \leq 2\beta_0$ if and only if

$$\gamma i_R(1-\rho\tilde{\iota}_R)(2\rho\tilde{\iota}_R - 1) \leq \rho\tilde{\iota}_R(1-i_R). \tag{52}$$

Since the right-hand side is always positive, recalling that $\rho\tilde{\iota}_R < 1$, the inequality is fulfilled for every $\gamma \in (0,1]$ when $\rho\tilde{\iota}_R \leq \frac{1}{2}$. If instead $\rho\tilde{\iota}_R \in \left(\frac{1}{2}, 1\right)$, then (52) is satisfied for $\gamma \leq \hat{\gamma}$, with $\hat{\gamma}$ defined in (23).

Thus, it holds that $\beta_{ns} \leq 2\beta_0$ occurs for every $\gamma \in (0,1]$ when $\rho\tilde{\iota}_R \leq \frac{1}{2}$, and for $\gamma \leq \hat{\gamma}$ in (23) when $\rho\tilde{\iota}_R \in \left(\frac{1}{2}, \hat{\rho}\right)$. Hence, the first system in (51) can be split as follows[9]

$$\begin{cases} i_R \in (0, \frac{2}{3}] \\ \rho\tilde{\iota}_R \leq \frac{1}{2} \\ \rho\tilde{\iota}_R < \hat{\rho} \\ \beta < \beta_{ns} \end{cases} \quad \vee \quad \begin{cases} i_R \in (0, \frac{2}{3}] \\ \gamma \leq \min\{1, \hat{\gamma}\} \\ \rho\tilde{\iota}_R \in \left(\frac{1}{2}, \hat{\rho}\right) \\ \beta < \beta_{ns} \end{cases} \tag{53}$$

Similarly, the second system in (51) can be split as follows

$$\begin{cases} i_R \in (\frac{2}{3}, 1) \\ \gamma \leq \frac{2(1-i_R)}{i_R} \\ \rho\tilde{\iota}_R \leq \frac{1}{2} \\ \rho\tilde{\iota}_R < \hat{\rho} \\ \beta < \beta_{ns} \end{cases} \quad \vee \quad \begin{cases} i_R \in (\frac{2}{3}, 1) \\ \gamma \leq \frac{2(1-i_R)}{i_R} \\ \gamma \leq \hat{\gamma} \\ \rho\tilde{\iota}_R \in \left(\frac{1}{2}, \hat{\rho}\right) \\ \beta < \beta_{ns} \end{cases}$$

However, since for $\rho\tilde{\iota}_R > \frac{1}{2}$ it holds that $\frac{2(1-i_R)}{i_R} < \hat{\gamma}$, the two systems above can be unified into

$$\begin{cases} i_R \in (\frac{2}{3}, 1) \\ \gamma \leq \frac{2(1-i_R)}{i_R} \\ \rho\tilde{\iota}_R < \hat{\rho} \\ \beta < \beta_{ns} \end{cases} \tag{54}$$

As concerns the third system in (51), it can be split as follows

$$\begin{cases} i_R \in (\frac{2}{3}, 1) \\ \frac{2(1-i_R)}{i_R} < \gamma \leq 1 \\ \rho\tilde{\iota}_R \leq \frac{1}{2} \\ \rho\tilde{\iota}_R < \hat{\rho} \\ \beta_{fl} < \beta < \beta_{ns} \end{cases} \quad \vee \quad \begin{cases} i_R \in (\frac{2}{3}, 1) \\ \frac{2(1-i_R)}{i_R} < \gamma \leq \min\{1, \hat{\gamma}\} \\ \rho\tilde{\iota}_R \in \left(\frac{1}{2}, \hat{\rho}\right) \\ \beta_{fl} < \beta < \beta_{ns} \end{cases} \tag{55}$$

Observing that $\hat{\rho} > \frac{1}{2}$ requires $\gamma > \frac{1-i_R}{i_R}$, we have that (53) can be rewritten as follows

$$\begin{cases} i_R \in (0, \frac{2}{3}] \\ \rho\tilde{\iota}_R \leq \frac{1}{2} \\ \rho\tilde{\iota}_R < \hat{\rho} \\ \beta < \beta_{ns} \end{cases} \quad \vee \quad \begin{cases} i_R \in (0, \frac{2}{3}] \\ \frac{1-i_R}{i_R} < \gamma \leq \min\{1, \hat{\gamma}\} \\ \rho\tilde{\iota}_R \in \left(\frac{1}{2}, \hat{\rho}\right) \\ \beta < \beta_{ns} \end{cases} \tag{56}$$

Combining the various possibilities for the validity of (54), (55) and (56), recalling (17) we obtain the desired result. □

[9]Direct computations show that, for $\rho\tilde{\iota}_R \in \left(\frac{1}{2}, \hat{\rho}\right) \subset \left(\frac{1}{2}, 1\right)$, it holds that $\hat{\gamma} \geq 1$ for $i_R \in \left(\frac{2}{3}, \frac{\rho\tilde{\iota}_R}{4\rho\tilde{\iota}_R - 2(\rho\tilde{\iota}_R)^2 - 1}\right]$, while $\hat{\gamma} < 1$ for $i_R \in \left(\frac{\rho\tilde{\iota}_R}{4\rho\tilde{\iota}_R - 2(\rho\tilde{\iota}_R)^2 - 1}, 1\right)$.

References

[1] M. Sharma, S. Mindermann, C. Rogers-Smith, G. Leech, B. Snodin, J. Ahuja, J. B. Sandbrink, J. T. Monrad, G. Altman, G. Dhaliwal, L. Finnveden, A. J. Norman, S. B. Oehm, J. F. Sandkühler, L. Aitchison, T. Gavenčiak, T. Mellan, J. Kulveit, L. Chindelevitch, S. Flaxman, Y. Gal, S. Mishra, S. Bhatt, J. M. Brauner, Understanding the effectiveness of government interventions against the resurgence of COVID-19 in Europe, Nat. Commun. 12 (2021) 5820.

[2] C. Murphy, J. Y. Wong, B. J. Cowling, Nonpharmaceutical interventions for managing SARS-CoV-2, Curr. Opin. Pulm. Med. 29 (2023) 184–190.

[3] J. Allen, D. J. Watts, D. G. Rand, Quantifying the impact of misinformation and vaccine-skeptical content on Facebook, Science 384 (2024) eadk3451.

[4] J. D. Sachs, S. S. A. Karim, L. Aknin, J. Allen, K. Brosbøl, F. Colombo, G. C. Barron, M. F. Espinosa, V. Gaspar, A. Gaviria, A. Haines, P. J. Hotez, P. Koundouri, F. L. Bascuñán, J.-K. Lee, M. A. Pate, G. Ramos, K. S. Reddy, I. Serageldin, J. Thwaites, V. Vike-Freiberga, C. Wang, M. K. Were, L. Xue, C. Bahadur, M. E. Bottazzi, C. Bullen, G. Laryea-Adjei, Y. Ben Amor, O. Karadag, G. Lafortune, E. Torres, L. Barredo, J. G. E. Bartels, N. Joshi, M. Hellard, U. K. Huynh, S. Khandelwal, J. V. Lazarus, S. Michie, The Lancet Commission on lessons for the future from the COVID-19 pandemic, Lancet 400 (2022) 1224–1280.

[5] Y. Huang, Q. Zhu, Game-Theoretic Frameworks for Epidemic Spreading and Human Decision-Making: A Review, Dyn. Games Appl. 12 (2022) 7–48.

[6] W. O. Kermack, A. G. McKendrick, Contributions to the mathematical theory of epidemics. II. —The problem of endemicity, Proc. R. Soc. Lond. A 138 (1932) 55–83.

[7] V. Piccirillo, Nonlinear control of infection spread based on a deterministic SEIR model, Chaos Solitons Fractals 149 (2021) 111051.

[8] V. Ambalarajan, A. R. Mallela, V. Sivakumar, P. B. Dhandapani, V. Leiva, C. Martin-Barreiro, C. Castro, A six-compartment model for COVID-19 with transmission dynamics and public health strategies, Sci. Rep. 14 (2024) 22226.

[9] T. C. Reluga, Game Theory of Social Distancing in Response to an Epidemic, PLoS Comput. Biol. 6 (2010) e1000793.

[10] I. Kordonis, A.-R. Lagos, G. P. Papavassilopoulos, Dynamic Games of Social Distancing During an Epidemic: Analysis of Asymmetric Solutions, Dyn. Games Appl. 12 (2022) 214–236.

[11] Y. Zhou, M. M. Rahman, R. Khanam, B. R. Taylor, Individual preferences, government policy, and COVID-19: A game-theoretic epidemiological analysis, Appl. Math. Model. 122 (2023) 401–416.

[12] K. M. A. Kabir, J. Tanimoto, Evolutionary game theory modelling to represent the behavioural dynamics of economic shutdowns and shield immunity in the COVID-19 pandemic, R. Soc. Open Sci. 7 (2020) 201095.

[13] A. R. Hota, U. Maitra, E. Elokda, S. Bolognani, Learning to Mitigate Epidemic Risks: A Dynamic Population Game Approach, Dyn. Games Appl. 13 (2023) 1106–1129.

[14] H. Zhang, Z. Sun, N. Zhao, Y. Liu, Government response, individual decision-making, and disease spreading: Insights from a game-epidemic dynamics model, Chaos Solitons Fractals 191 (2025) 115796.

[15] R. Tori, J. Tanimoto, A study on prosocial behavior of wearing a mask and self-quarantining to prevent the spread of diseases underpinned by evolutionary game theory, Chaos Solitons Fractals 158 (2022) 112030.

[16] A. Glaubitz, F. Fu, Social dilemma of nonpharmaceutical interventions: Determinants of dynamic compliance and behavioral shifts, Proc. Natl. Acad. Sci. U.S.A. 121 (2024) e2407308121.

[17] M. Noori, N. Azimi-Tafreshi, M. Salahshour, Coevolution of cooperation and epidemic spreading, Phys. Rev. Res. 7 (2025) 023211.

[18] D. Madeo, C. Mocenni, Evolutionary Game Theoretic Insights on the SIRS Model of the COVID-19 Pandemic, IFAC-PapersOnLine 54 (2021) 1–6.

[19] J. Hofbauer, K. Sigmund, Evolutionary Games and Population Dynamics, Cambridge University Press, 1st edition, 1998.

[20] D. Goforth, D. Robinson, The Topology of the 2x2 Games, Routledge, London, 1st edition, 2004.

[21] L. J. Allen, Some discrete-time SI, SIR, and SIS epidemic models, Math. Biosci. 124 (1994) 83–105.

[22] J. Hofbauer, K. Sigmund, Evolutionary game dynamics, Bull. Am. Math. Soc. 40 (2003) 479–519.

[23] F. Cavalli, A. Naimzada, M. Pireddu, D. Visetti, An Epidemiological Evolutionary Game: General Framework, Possible Lock-in States and Uncertainty, Technical Report 11, CISEPS Working Paper Series, 2026.

[24] L. Gardini, N. Schmitt, I. Sushko, F. Tramontana, F. Westerhoff, Necessary and sufficient conditions for the roots of a cubic polynomial and bifurcations of codimension-1, -2, -3 for 3D maps, J. Differ. Equ. Appl. 27 (2021) 557–578.